# Beam Bunch Length Measurement for the ARIEL e-LINAC

Alysson Vrielink

Sponsor: Robert Laxdal

ENPH 479

Engineering Physics

The University of British Columbia

Project Number 1269

January 16, 2013

# Executive Summary

The following document presents measurements conducted to determine and manipulate the beam bunch length in an electron linear accelerator at TRIUMF's new ARIEL facility. This method uses a radiofrequency resonant cavity that operates in a mode with transverse electromagnetic fields on axis. These fields deflect electrons by a magnitude dependent on the phase of the radiofrequency fields at the arrival time of the electron. Therefore, it is possible to convert the spread of electrons after the deflection to a profile of the beam in the time domain before it reached the deflecting cavity.

This relationship between bunch length and vertical spread after the deflecting cavity requires that certain properties of the cavity be measured. In particular, the effective shunt impedance must be known, a parameter that gives the relationship between input power and effective cavity voltage. To obtain this measurement, we look at the effect of the deflecting cavity on the beam and compare this with results obtained from simulations using a 3D beam dynamics program, General Particle Tracer. Preliminary results suggest the effective shunt impedance of the deflecting cavity is 0.81 M$\Omega$, however this should be confirmed with further data collection.

In addition to beam bunch length measurements, this project characterized the bunching cavity, a radio-frequency resonant cavity designed to focus the beam in the time domain. Using the bunching cavity in conjunction with the deflector cavity, we were able to measure the nominal bunching power for optimal focusing at the deflecting cavity to be 48.5W. When compared with computer simulations, the shunt impedance of the buncher was calculated to be 0.326M$\Omega$. Thiis shunt impedance can be used to determine the input power required for optimal temporal focusing of the beam at any point along the beamline. This is important as a focused bunch is highly desirable for downstream users.

As these results are only a first estimate, it would be useful to do further data collection to confirm these values and obtain error bounds. In addition, the computer simulations could be improved by using more recent estimates of the input beam characteristics (standard deviation of the bunch in the x, y and z directions, beam energy, etc...). Having obtained the most accurate results possible for the shunt impedance of the deflecting cavity, a final recommendation would be to develop a program that can rapidly analyze images of the beam after the deflector and output the beam bunch length.

# Contents

# List of Tables

# List of Figures

# List of Abbreviations

| | |
|---|---|
| TRIUMF | TRI-University Meson Facility |
| ARIEL | Advanced Rare IsotopE Laboratory |
| VECC | Variable Energy Cyclotron Center (Kolkata, India) |
| e-LINAC | Electron Linear Accelerator |
| GPT | General Particle Tracer (3D Simulation Software) |
| DB1 | Diagnostic Box 1 |
| RF | Radio-Frequency |
| SRF | Superconducting Radio-Frequency |
| NIM | Non Intercepting Monitor |
| FFC | Fast Faraday Cup |
| ERL | Energy Recovery Linac (Cornell) |
| GUI | Graphical User Interface |
| BPM | Beam Profile Monitor |
| FC | Faraday Cup |
| HP Slit | High Power Slit |

# Chapter 1

# Background and Motivation

## 1.1 The ARIEL Project

TRIUMF, Canada's national laboratory for particle and nuclear physics, is entering an exciting new phase with the upcoming completion of the Advanced Rare IsotopE Laboratory (ARIEL) project. This facility will triple TRIUMF's current capability for producing rare isotope beams used by researchers in fields ranging from astrophysics to materials engineering to particle physics, as well as in cancer treatment and radiation therapy. This will be accomplished by the installation of a 50MeV, 10mA continuous wave electron linear accelerator (e-LINAC) that will operate using highly efficient superconducting radiofrequency technology[1].

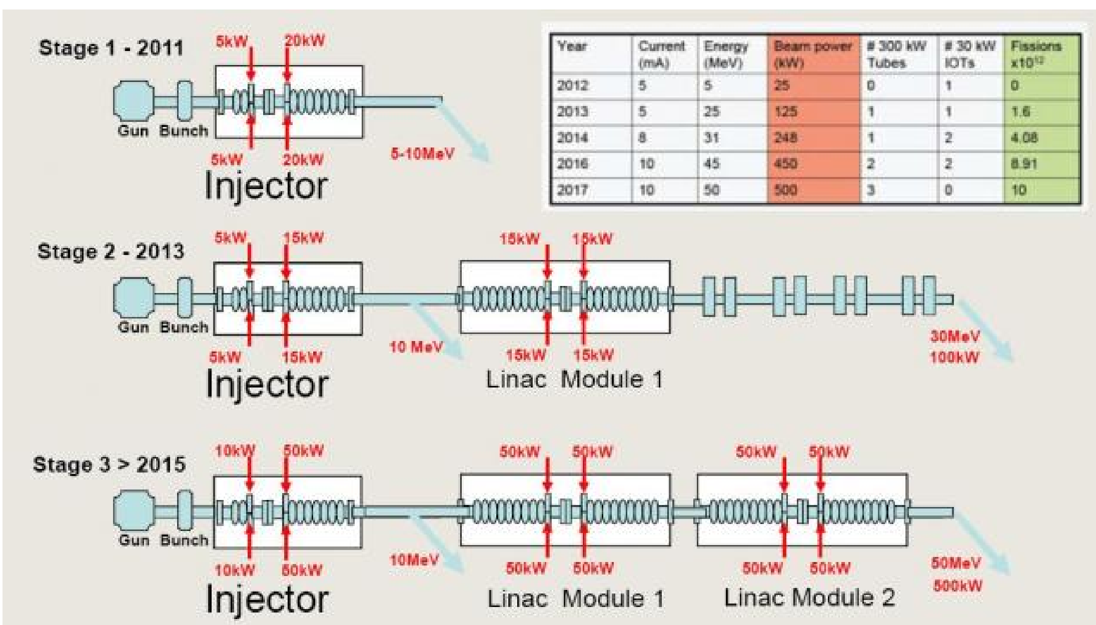


Figure 1.1: An overview of the E-LINAC project

[1] http://www.triumf.ca/ariel/e-linac

### 1.1.1 The e-LINAC

The first stages of the e-LINAC project are already well under way as TRIUMF works with collaborators from the Variable Energy Cyclotron Center (VECC) in Kolkata, India to commission the injection line. This injection line will be used to emit and accelerate the electrons up to relativistic speeds necessary for optimal acceleration in the superconducting resonant cavities. As pictured in figure 1.2, the injector consists of a thermionic electron gun (on the far left), followed by several devices to focus and steer the beam, as well as diagnostic devices to determine beam characteristics. The electrons are emitted from the electron gun in bunches with a length that depends on the cathode bias of the gun. Electrons will only be emitted from the gun when the sinusoidal RF gun voltage is higher than the cathode bias. This phase window is called the conduction angle.

From the gun, the beam proceeds downstream until it reaches the dipole magnet, shown as a rotated green box in figure 1.2, where depending on the state of the magnet, the beam will either be bent 90° into the analyzing leg of the injection line, or will continue straight through to the end of the line. While the beam currently stops at a beam dump on the far right, as other stages of the accelerator are completed, the beam will continue through to the next stage (i.e. the accelerating cavities).

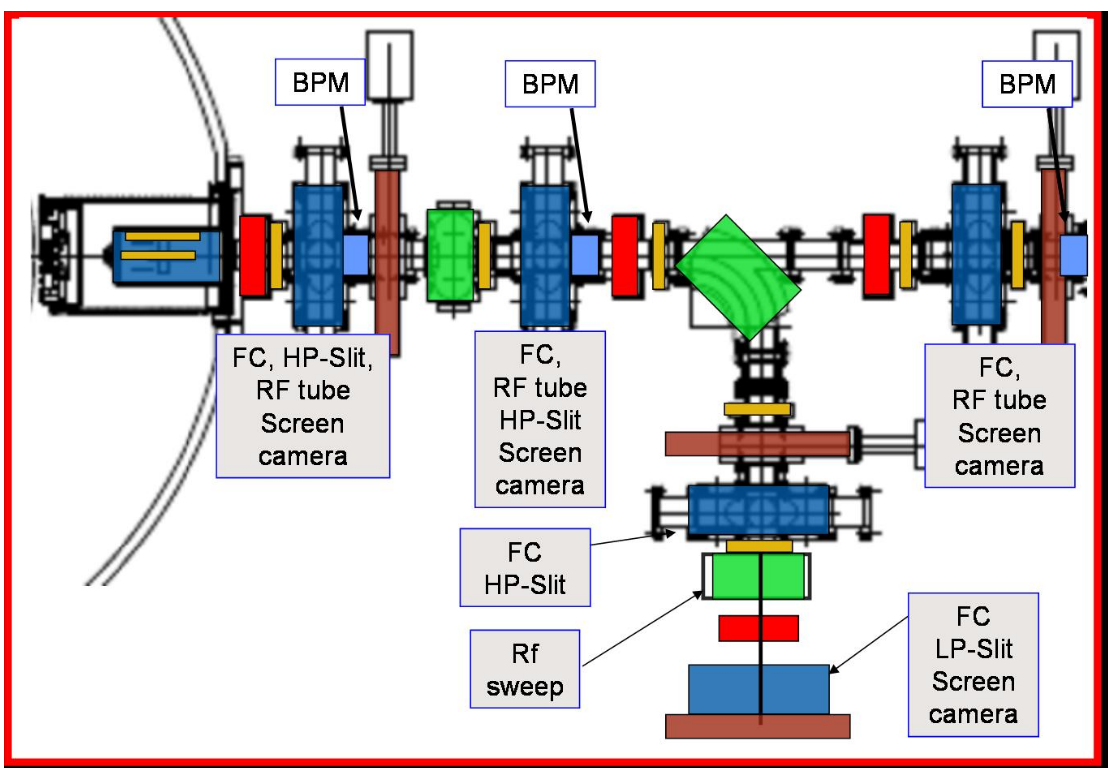


Figure 1.2: A diagram of the injector line for the ARIEL e-LINAC

## 1.2 Beam Diagnostics

Apart from ensuring the beam is of a high enough energy, an important consideration for accelerator engineers is the quality of the beam reaching the downstream users. Diagnostic devices are interspersed along the injection line that allow us to measure characteristics of the beam such as the cross sectional distribution of the beam in the $x-y$ plane and the average beam current. Characteristics that are not as easy to measure include the temporal distribution of the beam as well as its canonical conjugate, the energy distribution of the beam. Having a beam that is focused in time and with small energy spread is as important as obtaining a small cross sectional area.

### 1.2.1 Bunch Length Measurement

With a bunch length on the order of 85 picoseconds long, it would require a very high resolution device to analyze the beam in the time domain. There are devices installed in the beamline that are capable of very high sampling rates, such as a fast faraday cup which outputs a current proportional to the rate of electrons hitting the cup. This current is converted to a voltage and sampled by a high speed digital oscilloscope. Another possible method of determining the bunch length is using a non intercepting monitor (NIM) that picks up the harmonic content of the beam. From this signal, one can measure not only the bunch length, but also the phase of the electrons in the bunch relative to the gun RF phase. Both of these options have been tested in conjunction with an RF bunching cavity that focuses the beam in the longitudinal direction (i.e shortens the time spread of the bunch). Unfortunately, the fast faraday cup does not produce a reliable signal without very high beam current, while the NIM installed in the injector can not sample quickly enough to give anything other than the average phase content of the beam.

### 1.2.2 The Deflecting Cavity

Fortunately, there is a third device that has been designed specifically for these measurements. Pictured in green and labeled RF Sweep in figure 1.2, the low power, room temperature deflecting cavity is a resonant cavity that deflects electrons depending on their arrival time. The transverse electromagnetic fields inside the resonant cavity have a time dependence, resulting in the electrons experiencing different forces depending on the RF phase of the cavity when the electron enters. Essentially, this device maps from the time domain to the space domain, where we already have several high resolution devices capable of measuring the beam position and profile.

The deflecting cavity for the ARIEL e-LINAC, pictured installed in the analyzing leg of the injector line in figure 1.3, was commissioned over the summer. However, to utilize the cavity as a means of determining the bunch length measurement, we must know the relationship between the arrival time of an electron

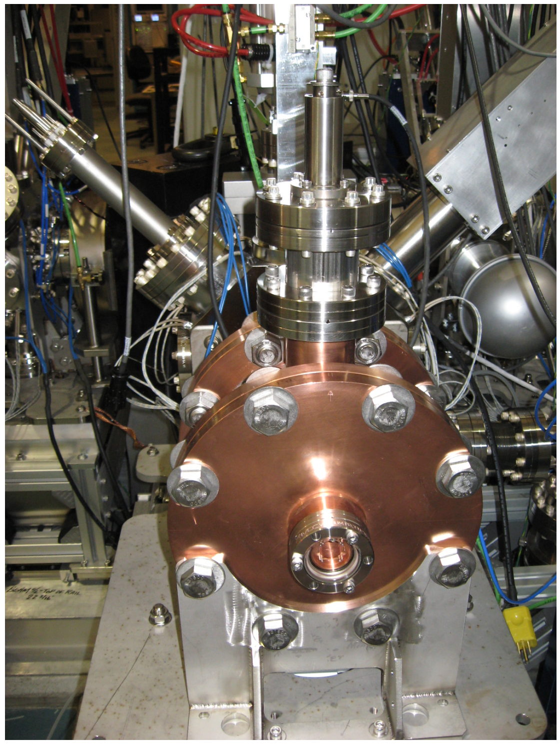

Figure 1.3: The deflector cavity installed in the injector line

at the cavity, and its position in the $x - y$ plane at the diagnostic box on the end of the analyzing leg (pictured in blue in figure 1.2). This relationship depends on several factors, including the RF characteristics of the deflecting cavity, the input power to the cavity, the energy and position of the beam when it reaches the cavity and the focusing elements in place after the cavity. Indeed, the relationship is significantly complicated by a solenoid focusing element in between the deflector and the measurement point (shaded in red); this solenoid is necessary to collimate the beam before the diagnostic box but couples the x and y elements of the beam trajectory. This results in a rotated x-y axis after the solenoid, evident on the screen at DB1.

The main characteristic of the deflecting cavity that needs to be determined to obtain the relationship between vertical spread and bunch length is called the shunt impedance of the cavity. This gives us the relationship between input power to the cavity (known), and the effective voltage of the cavity (unkown). If we know the effective deflecting voltage, we can determine the energy imparted to an electron in the y direction, and from this we can get a relationship between vertical spread and bunch length. Theoretically, this value can be calculated from RF simulations using programs such as CST Microwave Studio, however due to differences in the actual constructed cavity and the computer model, the shunt impedance needs to be measured.

$$P_{cavity} = \frac{V^2}{R_{sh}} \tag{1.1}$$

### 1.2.3 Bunch Energy Spread Measurements

We have discussed how to obtain the bunch length of the electron beam, but as mentioned, the energy spread of the beam is equally important. This is also a measurement that is difficult to obtain using standard diagnostic devices, but a clever method of measuring energy spread has been built directly into the accelerator design. The analyzing leg has specifically been placed at a 90 degree angle, with a dipole magnet used to direct the beam.The magnet will bend the trajectory of the electron with a radius of curvature given by equation 1.2, where B is the magnetic field of the dipole magnet, $m_0$ is the rest mass of an electron and $q$ is the charge of an electron.

$$R = \frac{\gamma m_0 \beta c}{qB} \tag{1.2}$$

Depending on the energy of the electron (represented by $\gamma$ in equation 1.2), the radius of curvature of the electron will change and thus the trajectory after the dipole magnet will be related to the electron's energy before the dipole. In particular, because the magnet is bending the beam in the x direction, an energy spread before the dipole magnet will map to a spread in the x direction after the dipole. Similarly to the deflector cavity mapping from the time domain to the space domain (y direction), the dipole magnet is mapping from the energy domain to the space domain (x direction). Figures 1.4 and 1.5 demonstrate this concept, showing simulations of a beam going through the dipole magnet with and without a large energy spread.

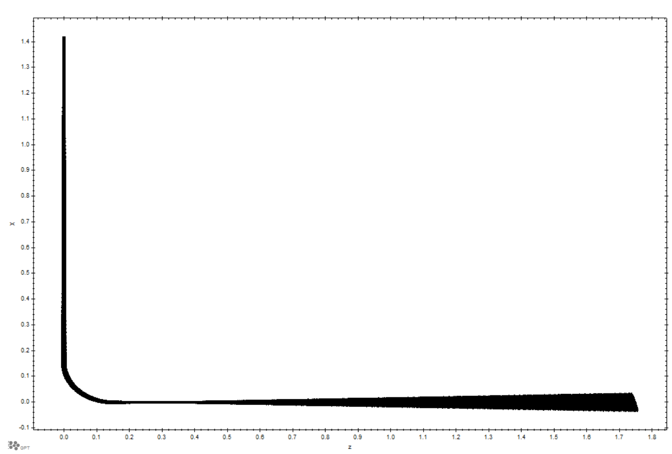

Figure 1.4: A beam bending through the dipole magnet with small energy spread. The y axis represents the x direction, and the x axis represents the z direction (direction of travel of the beam after the dipole).

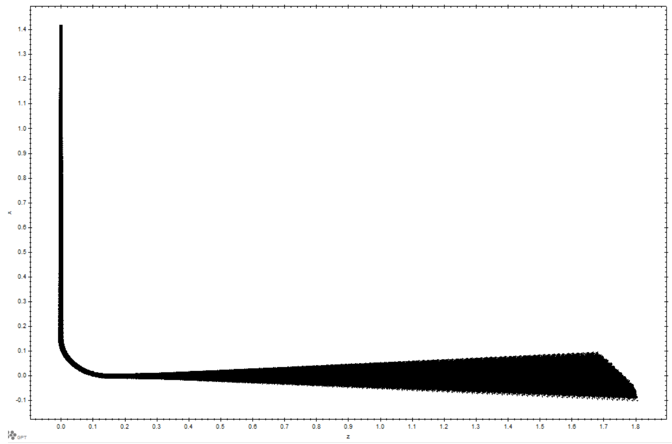

Figure 1.5: A beam bending through the dipole magnet with energy spread 100 times larger than in the previous figure. The spread in the x direction (y axis) is much larger after the dipole.

Therefore, we can measure the spread in the x direction using the diagnostic box at the end of the analyzing leg, represented by a brown rectangle in figure 1.2, and use this measurement to determine the energy spread of the beam before it reached the dipole magnet.

### 1.2.4 The Buncher Cavity

There is one final element in the injector beamline that is very important when considering both the time and energy spread of the beam. The buncher cavity, depicted in figure 1.2 by the first green rectangle on the left, is a radiofreqency room temperature resonant cavity that is designed to focus the beam bunches in time. It does this by slowing down electrons at the front of the bunch and accelerating electrons at the back of the bunch. This is accomplished using a sinusoidal RF field, such that depending on the time of arrival of the electron, it will experience a different phase of the RF as it passes through the resonant cavity.

For the buncher to properly focus, it must be operated at the correct phase, as shown in figure 1.6, called the bunching phase. If operated $\pm 90°$ away from the bunching phase, the bunch will experience a maximum net acceleration or deceleration while if operated at $180°$ away from the bunching phase, fast electrons will be accelerated and slow electrons further decelerated causing an increase in the time spread of the bunch (this is the debunching phase).

It is important to note that in bunching the beam, the buncher reduces the spread in time but in doing so, imparts further energy spread in the beam. A more detailed discussion of the buncher cavity RF and determination of the optimal buncher power can be found in Appendix A.

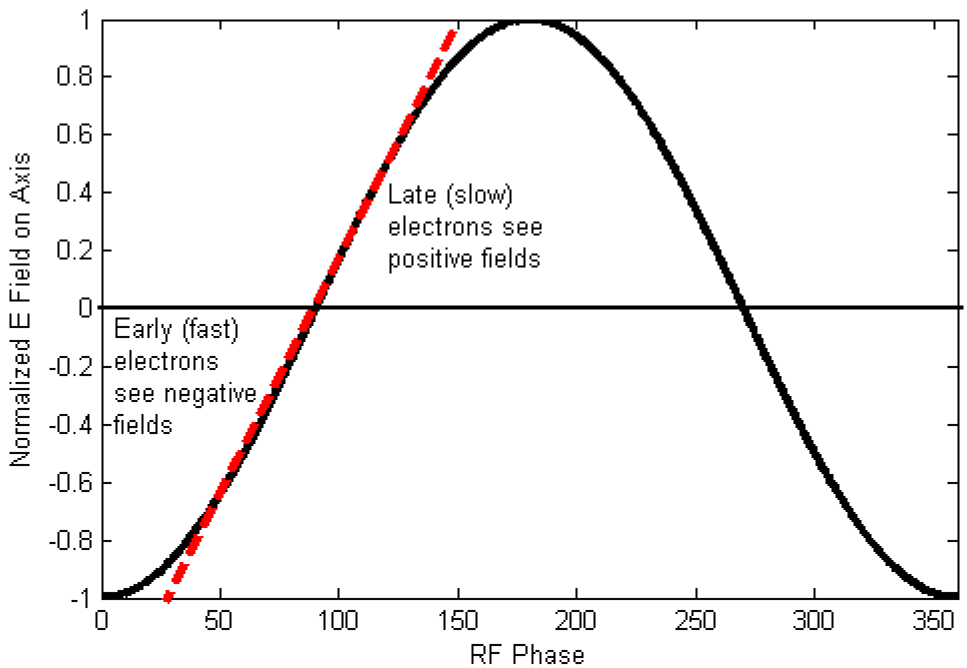


Figure 1.6: A sinusoid depicting the fields in an RF bunching cavity. The middle of the bunch reaches the cavity at the zero crossing point while electrons arriving at a later phase (lagging) undergo acceleration and electrons arriving at an earlier phase (leading) undergo deceleration.

## 1.3 Beam Dynamics Simulations

In the preceding sections, we have discussed the importance of knowing the time and energy spread of our bunched beam as well as the tools required to convert these parameters into the space domain, where they can be measured. These tools consist of the deflecting cavity and a dipole, used to map from the time and energy domains respectively. We also have access to a buncher cavity designed to focus the bunch in the time domain at the expense of increasing the energy spread.

As we can see from figure 1.2, the aforementioned devices are not the only elements acting on the beam. There are also focusing solenoids, magnetic steerers and collimators used to remove electrons that are too far from the center of the beam in the radial (x-y) direction. All of these devices will affect the beam profile and must be taken into account when determining the time and energy spread from the y and x spread of the beam.

As the factors mentioned above depend on design parameters unique to the e-LINAC, there is clearly no off-the-shelf solution to this problem but rather a model must be derived from first principles where possible, and the results of computer simulations. Fortunately, while the exact beam optics set-up is unique, modeling beam dynamics is a common problem and there are numerous 2D and 3D computer simulations to model beam dynamics [5, 2]. In addition, the use of deflector cavities is fairly common in accelerator engineering and there are several papers discussing methods of measuring the longitudinal beam profile from the deflection of the individual particles. The TRIUMF e-LINAC deflecting cavity is based off a design used by Cornell which has considerable documentation ([1, 4, 3]) regarding bunch length diagnostics and beam dynamics using the code, General Particle Tracer (GPT) [2].

While the codes already exist, it is not necessarily straightforward to solve for the trajectory; all of the input parameters must be defined, and if more than one code is necessary to simulate the multiple features in the beamline, it will be necessary to merge the simulation results. As the parameters also change depending on the operating conditions (beam current, beam energy, etc...) this model must be versatile, with the option to easily adjust such parameters. For this project, the RF fields for the buncher and deflector cavities were simulated using CST Microwave Studio, and then these fields were used in a GPT simulation that modeled the entire injection line up to the diagnostic box at the end of the analyzing leg.

This beam dynamics simulation in GPT can be used to compare with results obtained experimentally, and useful information regarding the RF cavities as well as beam characteristics can be obtained.

## 1.4 Project Objectives

The main purpose of this project is to provide accelerator engineers and downstream users of the ARIEL project with a rapid and straightforward method of determining the electron beam bunch length of the e-LINAC. This will be in the form of a MATLAB program that takes input parameters such as the RF characteristics and input power of the deflecting cavity, and the current of the solenoid. It will then uses the raw data obtained from the diagnostic box after the deflector cavity to output the bunch length.

There are varying degrees to which this program can be implemented, with the final objective being a one-click solution where the program interfaces with the existing framework to obtain all required input parameters and measurement data. However, the scope of this project will be limited due to time constraints and most likely will not reach that level of functionality.

The following list shows what this project expects to accomplish by the middle of January, 2013:

[2]http://www.pulsar.nl/gpt/

**USER INPUTS**

- Deflector Cavity Shunt Impedance, Q factor and Input Power
- Solenoid Current
- RF Gun Voltage (Initial electron energy)
- Field of the bending dipole magnet
- Conduction Angle
- Beam position measurements after the deflector

**PROGRAM OUTPUT**

- The length of the bunch $\pm 5$ ps
- The energy spread of the bunch $\pm 1$ keV
- A profile of the beam in the time domain, in the form of a graph of beam current vs. longitudinal position (if possible)

## 1.5 Project Scope and Limitations

The preceding section outlined the intended project objectives, however as the project progressed it became clear that this would be well beyond what could be accomplished by one individual given the time constraints at hand. In addition, while the original objectives focused only on the deflector cavity, the final project includes analysis of the bunching cavity as well.

Although the computer application described above ended up being outside the scope of this project, significant progress was made in characterizing the RF cavities of the injection line so that it would now be possible to continue with such a program. Several of the following accomplishments were required before the primary objective, given in section 1.4, could be addressed. There are also several that pertain to the bunching cavity which were not included in the original project scope.

- Determined the optimal beam optics set-up for measuring the time and energy spread of the beam bunches
- Developed operating procedures for the buncher and deflector cavity
- Worked on the experimental set-up (the injection line) so that data could be collected. This was more involved than was expected, and due to several projects underway in the VECC area, it was difficult to maintain the experimental set-up in the configuration necessary for our data collection.
- Provided quantitative and qualitative evidence that the buncher and deflector cavity were working as expected
- Determined the RF characteristics of the buncher and deflector cavity as installed in the injection line including power losses through the input cables

and the shunt impedance of the cavities, which is the most important quality in determining the relationship between effective voltage and input power

- Developed, in collaboration with members of the beam optics group and collaborators from VECC, a model of the injection line in General Particle Tracer, a 3D computer simulation software.

# Chapter 2

# Discussion

## 2.1 Experimental Set-Up and Data Collection

To fully characterize the RF devices (buncher and deflector), we needed to look at their effect on the beam. This was done by running beam in the injection line and comparing the output of the diagnostics at various RF power levels and phases. The buncher and deflector were tested separately, looking solely at the effect of one while the other was turned off, and then finally the deflector was used in combination with the buncher to determine the nominal bunching power. Figure 2.1 shows the injection line, highlighting the RF devices that were adjusted, as well the diagnostic box where the data was collected; we chose this diagnostic box, DB1, as it is the only one that placed after all of the devices in question, including the dipole magnet.

### 2.1.1 Beam Optics

While eventually the intent is to use the buncher and deflector to adjust and probe the beam, for this experiment we are essentially doing the opposite, using the beam to probe the RF devices. As such, the first aspect of setting up the experiment was to tune the beam optics (devices used to steer and focus the beam) so that the beam had a very small emittance (tightly focused) before the deflector cavity. This is necessary for several reasons; in particular, if the beam isn't tightly focused as it passes through the deflector, electrons far from the reference trajectory will see fields that are considerably different than the on axis fields. This will skew the results obtained at DB1. In addition, if we are trying to compare the beam spread in the x and y directions after the deflector, we want these values to be very small so that the effect of the deflector will be more noticeable.

We obtained a tightly focused beam by adjusting the solenoid settings (solenoids are shown in red in figure 2.1) and by placing two collimators in the beamline before the dipole magnet. These collimators consist of a thin strip of metal with two slits at 90 degree angles, and a small hole with a 1mm radius, as shown in figure 2.2. The collimator is inserted into the beamline in such a way that it blocks the beam, with a small portion of the beam passing through one of the slits or the

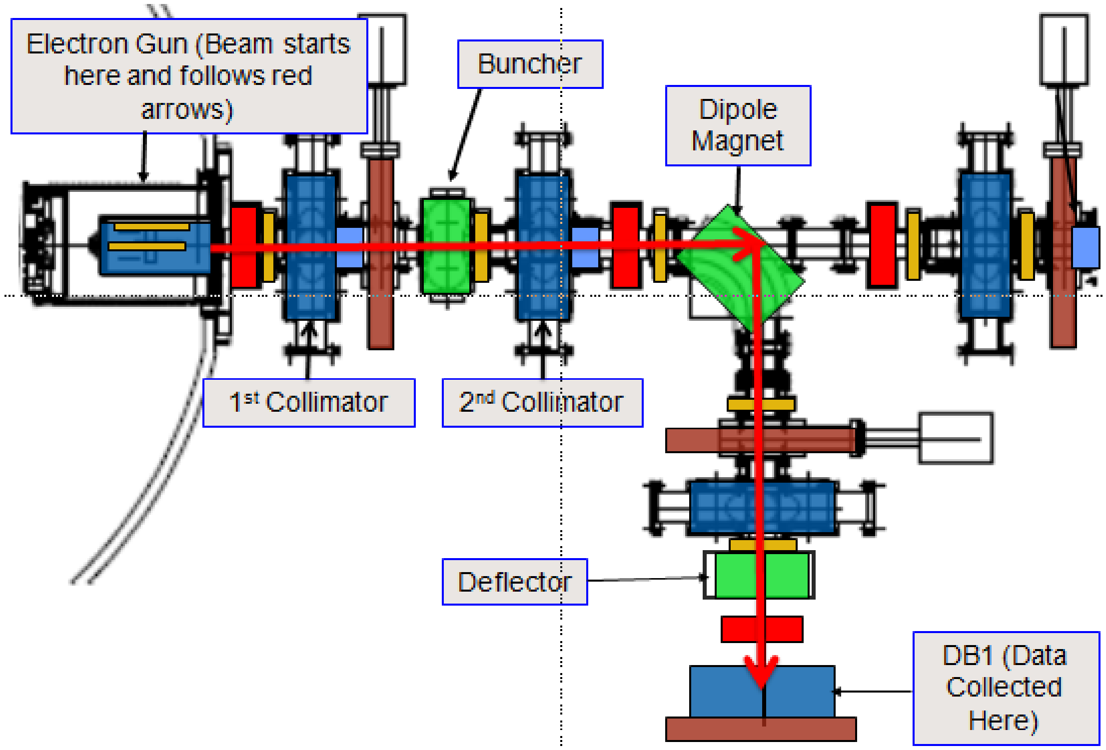


Figure 2.1: The experimental set-up.

hole in the middle, depending on the position of the collimator. By placing the hole in the center of the beamline, we limited the beam size at the collimating point to a radius of 1mm, blocking off any electrons that were further from the reference trajectory.

The beam optics settings, i.e. the current drawn by the steering and focusing elements, were saved and are attached in Appendix B. Note that the dipole magnet current setting is incorrect as it is no longer controlled by the VECC user interface, but by an external power supply. The setting for the dipole magnet was approximately 170mA, although this is not necessarily repeatable as work has been done on the dipole magnet since the data was collected.

### 2.1.2 Experimental Procedure

Having completed the experimental set-up, data collection could begin. Data was collected on several occasions, and this data was used to ensure the buncher and deflector were properly connected and the low level RF was functioning correctly. The data collected earlier in the project was also used to develop a final experimental procedure, answering questions such as how the beam should be set-up and whether or not the focusing solenoid after the deflector was necessary. The project supervisor, Bob Laxdal, wrote the majority of the final experimental procedure, however I have attached it in Appendix C for completeness. I have also revised this experimental procedure to accurately reflect the process used during the most recent round of data collection on November 26, 2012, which is

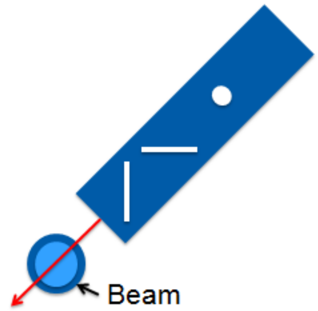


Figure 2.2: Depending on the depth of insertion (collimator enters on a 45 degree), the beam will pass through one of the slits or the hole, reducing the beam size to the shape of the collimating slit or hole.

the primary data set that will be discussed in this report.

Summarizing the experimental procedure, the first goal is to set up the beam correctly, as discussed in the previous subsection. The deflector can then be set up with the buncher off; this includes finding an input power that provides a reasonable vertical smear on the screen at DB1, and determining the phase which produces no deflection, and max deflection (0 degree phase). Having set up the deflector it should be turned off and the buncher can be configured, which includes determining the accelerating and decelerating phases, at 90 degrees to the bunching and debunching phases. The bunching phase can be determined by turning on the deflector at the predetermined operating power and deflecting phase, and identifying the buncher phase at which the vertical spread is minimized. The optimal bunching power, at which point the beam is maximally focused in time at the deflector, can be determined by slowly increasing the buncher power and determining the point at which the vertical spread in the beam at DB1 is minimized. At some point the beam spread will start increasing because the buncher is overfocusing in which case the beam is optimally focused in time at a point closer to the buncher than the deflector. Using the analogy of the human eye, overbunching is equivalent to nearsightedness, with the eye focusing light before the retina.

Data was collected with the deflecting cavity at a forward power of 17W. Considering the 3dB loss in the input cable this actually corresponds to a cavity input power of 8.52W. This is less than the expected nominal power of around 20-50W depending on bunch length, which is probably due to the time spread being much greater than expected as the gun was not specifically set-up to output a beam with short bunch length. Space charge would also increase the amount of deflection obtained at a given input power and bunch length.

The conduction angle (bunch length) could have been reduced by increasing the cathode bias. In our case, we ran the cathode bias at 101V, while it has been operated at voltages exceeding 240V. For this test, however, a small time spread was not needed as we were solely interested in measuring it, which is possible

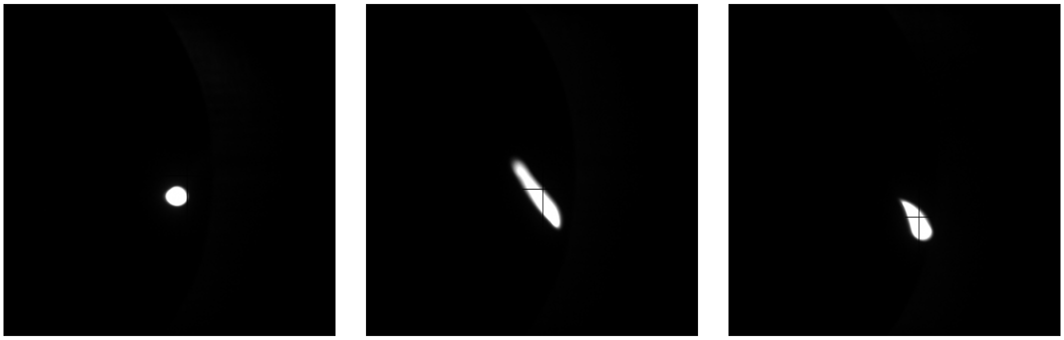

(a) Beam with no RF devices on (b) The deflector at maximum deflecting phase (0°) (c) The deflector at the peak amplitude phase (90°)

Figure 2.3: Effect of the Deflector Cavity on the Beam at DB1

as long as the bunch length is significantly less than one period of the deflector RF. The buncher was then turned on, with the deflector off, to a forward power of 15W. Accounting for the 1dB loss in the input cable, this corresponded to a cavity power of 11.9W. The bunching phase was identified, and with the deflector on at 8.5W forward power, the nominal power could be determined. The collected data was then analyzed, and the results are discussed in the following subsection.

### 2.1.3 Data Analysis and Results

#### The Deflecting Cavity

As discussed in the introduction, the purpose of the deflector cavity is to map from the time domain to the space domain; we therefore expect that by turning the deflector on, the vertical spread of the beam will increase significantly, reflecting the fact that the bunch is spread out in time. This was very clearly demonstrated in the collected data with the deflector on at 8.5W. Figure 2.3 compares pictures of the beam at the screen at DB1 with and without the deflector on (in all cases the bunching cavity is off).

Note that in this figure, particularly 2.3(b), the spread is not perfectly in the y direction but on an angle. As mentioned in section 1.2.2, the focusing solenoid after the deflector cavity rotates the x-y axes. While the spread induced by the deflector is really only in the y direction, it appears on an angle because of the effects of the solenoid. Through image processing of the data collected for the deflector and buncher in Matlab, it was determined that the coordinate system is rotated by approximately 36 degrees with the solenoid operating at 1.3A.

Figure 2.3 also demonstrates the effect of the deflector operating phase on the beam. As explained earlier, it is because the RF fields have a sinusoidal time dependence that the deflection is a function of time, and this is what provides the spread in the y direction. However, this also means that average deflection seen by the bunch will be a function of the RF phase at which the center of the bunch reaches the deflecting cavity. In figure 2.3(b) the deflector is operating such that the middle of the bunch reaches the deflector at the 0 degree phase so the center electrons experience no net deflection. Comparatively, in figure 2.3(c) the deflector is operating such that the middle of the bunch reaches the deflector at the 90 degree phase. At this point, there isn't much spread in the y direction because the top of a sinusoid is relatively flat (ie, electrons at the extremities of the bunch experience very similar fields to the center of the bunch). As a whole, the bunch experiences maximum deflection, which explains why we see a relatively focused beam with y centroid at a maximum distance from the y centroid with the deflector off.

The phase dependence is clearly illustrated in figure 2.4, where the rotated (solenoid coupling taken into account) y centroid of the beam is plotted as a function of deflector phase offset. In this figure the phase is relative to the electron gun RF, so is somewhat arbitrary. Clearly from this plot we can identify that the maximum deflecting phase (0 degree) occurs at approximately -90° and 100° according to the low level RF phase relative to the electron gun. Note the low level RF period isn't exactly 360° as it should be, meaning that changing the phase by 1 degree on the user interface changes the actual RF phase by slightly less than 1 degree.

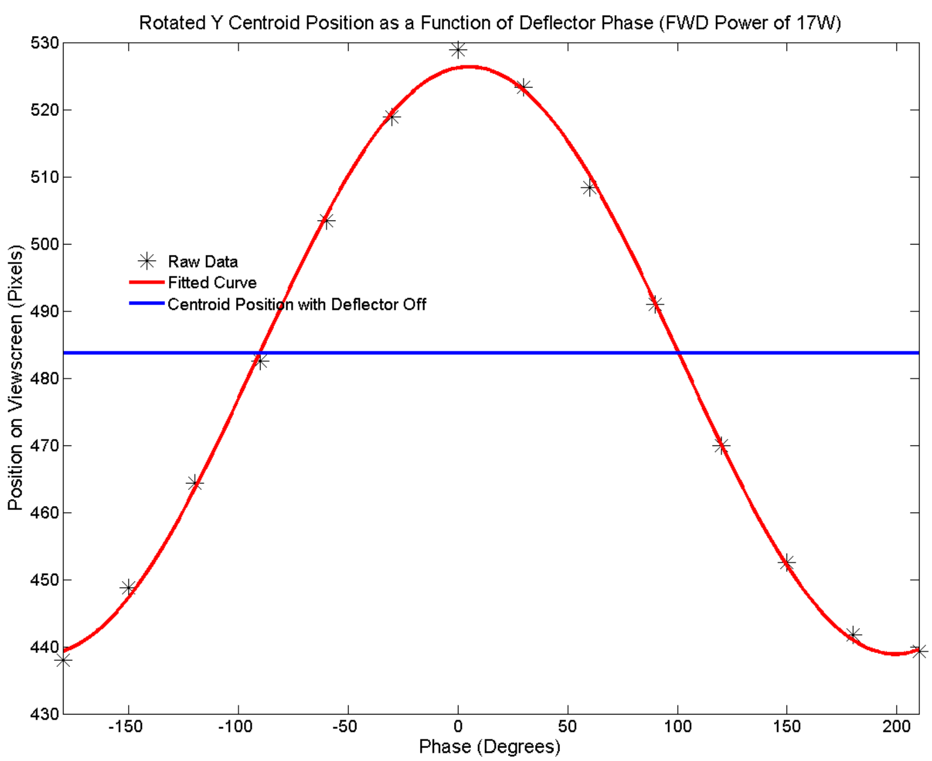


Figure 2.4: The rotated y centroid position (in pixels) as the deflector phase is scanned.

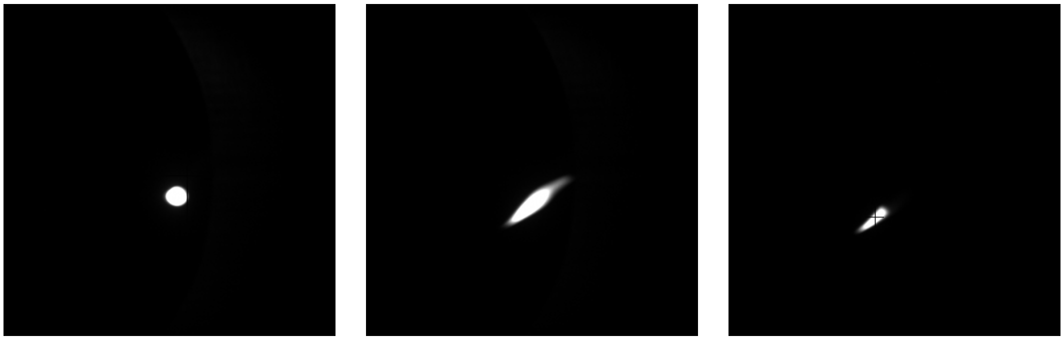

(a) Beam with no RF devices on

(b) The buncher at a non accelerating (bunching or de-bunching) phase

(c) The buncher at an accelerating phase

Figure 2.5: Effect of the Bunching Cavity on the Beam at DB1

### The Bunching Cavity

Similarly to identifying the deflecting phase of the deflector cavity, the first objective when running the buncher was to determine the bunching phase, as depicted in figure 1.6. The effect of the buncher on the beam at the screen at DB1 is shown in figure 2.5. Figure 2.5(b) is clearly one of the non accelerating phases (either the bunching or de-bunching phase), but we cannot determine which without operating the deflector as the image does not give us any information about the time spread.

We can identify the phase as being fairly close to the non-accelerating phase because the x centroid is in approximately the same position as the x centroid with the buncher off, which is what we'd expect when the buncher is operating at a zero crossing point. Because the slope of a sinusoid is maximum at the zero crossing point, we would also expect to see a beam that is very wide in the x direction as the spread in energy imparted by the buncher is greater at this phase. This larger energy spread manifests itself as a horizontal smear due to the effect of the dipole (section 1.2.3). Once again, due to the solenoid coupling, the axes are rotated, so the smear actually appears on an angle of around 36 degrees.

Contrasting the non accelerating phase, figure 2.5(c) shows the beam when the buncher is operating in one of the maximum accelerating phases. We can most likely identify this as the maximum deceleration phase because the center of mass is on the left of the reference beam (figure 2.5(a)), suggesting the beam had a smaller radius of curvature than the reference trajectory. From equation 1.2, this implies the beam had a lower energy. Another trait of the maximum accelerating phases is that the spread in energy imparted by the buncher will be significantly less because the slope of a sinusoid is at a minimum when the amplitude is at a maximum. In comparing the beam in figure 2.5(c) with figure 2.5(b), we can see that there is significantly less spread in the rotated x direction.

The sinusoidal dependence of the x centroid position on the buncher phase when the electrons arrive at the cavity can be seen quantitatively in figure 2.6. We can identify the non accelerating phases from the fitted curve with more accuracy than by looking solely at the images. These phases occur at the intersect of the red and blue lines, at approximately 180° and -10°. These are not 180 degrees apart, as we would expect, which is due to the fact that there is clearly a slight constant offset, such that the average of the buncher x centroid position is not quite the same as the the centroid position of the reference beam. The actual non accelerating phases are therefore closer to 175° and -5°.

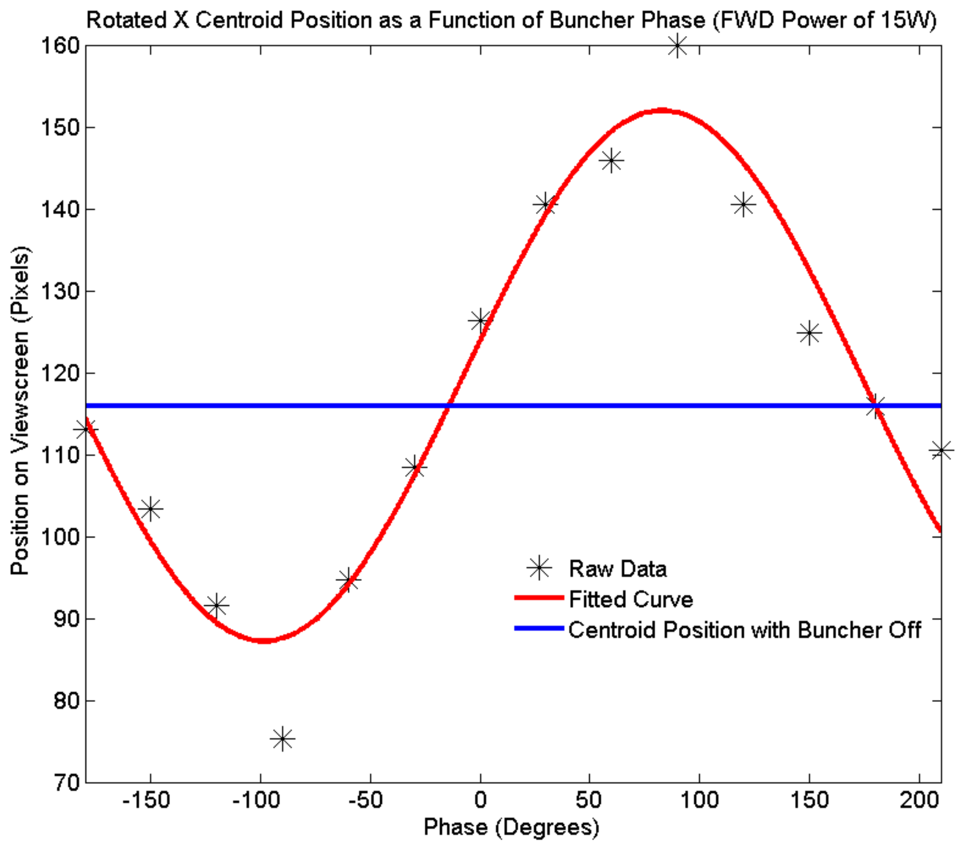


Figure 2.6: The rotated x centroid position (in pixels) as the buncher phase is scanned.

Having identified the non accelerating phases, the deflector needed to be turned on to determine the bunching phase. When collecting the data we used -98 degrees as our deflecting phase, which is very close to the -90 degree deflecting phase identified in figure 2.4. Therefore, in determining the bunching phase and nominal buncher power, we turned the deflector on at a power of 17W forward (8.5W with losses) and phase of -98° . We were then able to identify that the buncher phase was approximately $-20°$, close to the -5° expected from figure 2.6. The effect of turning on the buncher at a forward power of 14.2W (cavity power of 11.3 W after input losses) is shown in figure 2.7.

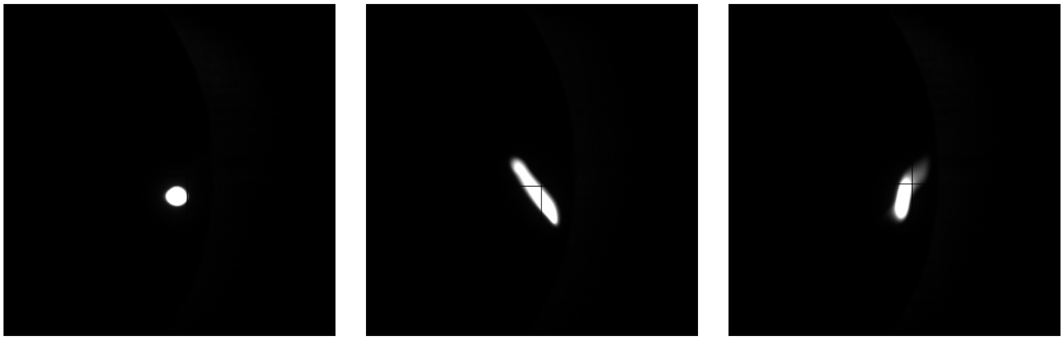

(a) Beam with no RF devices on

(b) Deflector at 8.5W and -98°

(c) Deflector at 8.5W and -98° and buncher at 11.3W and −20°

Figure 2.7: Effect of bunching on the deflector induced vertical smear at DB1

Keeping in mind that the solenoid is still rotating the axes, we can see that the buncher has significantly decreased the vertical smear evident when only the deflector is on, in figure 2.7(b). However, in doing so, the x spread of the beam has increased, as expected due to the increased energy spread imparted by the buncher cavity. This reciprocity between reducing the time spread and increasing the energy spread is due to what is known as Liouville's theorem, which states that the phase space volume of a system of particles is constant in time. As time is the canonical conjugate of energy, by decreasing the spread in time, Liouville's theorem implies there must be an increase in the spread in energy.

Having determined the bunching phase, the final step was to identify the nominal bunching power. This was done by keeping the deflector and buncher at the same settings described above, but by slowly increasing the buncher power, taking screenshots of the screen at DB1 throughout. The nominal bunching power will be the point at which the spread in time of the bunch is at a minimum, implying the length of the beam in the y direction is also minimized. Using Matlab to conduct image processing on the data collected, figure 2.8 was produced, showing a minimum in the y spread at a setpoint of approximately 450, corresponding to a buncher power of 61.1W (48.5W including losses). Returning to Liouville's theorem, figure 2.9 shows a maximum in the energy spread (x spread at DB1) at the same setpoint.

From this analysis, it is clear that the experimentally determined nominal bunching power is approximately 48.5W ± 5W. Compared to the theoretically calculated nominal power of 5W, determined in Appendix A, this is significantly higher. There are several factors that contribute to the increased actual buncher power. Space charge makes it more difficult to focus the beam as the electrons are repelling each other. In addition, the trajectory of the electrons depends on the energy imparted by the buncher and the time of arrival at the deflector will vary depending on the path the electron takes (this is not considered in my theoretical analysis). Finally, the fact that there is already energy spread in the beam when it

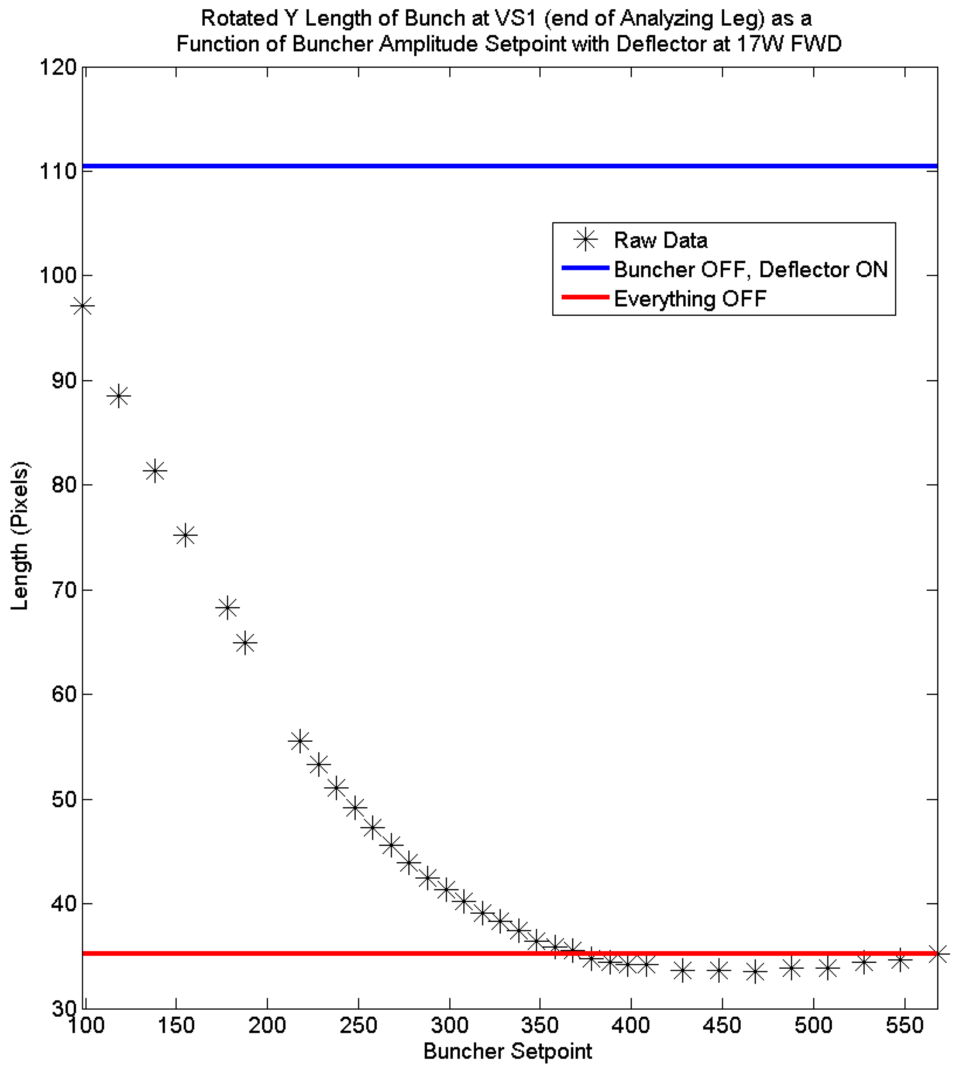


Figure 2.8: The rotated y length (in pixels) as the buncher phase is scanned.

reaches the buncher is not taken into account in the theoretical analysis, but could play a role in increasing the required bunching power. An electron that reaches the buncher first will probably have a higher energy, so even in slowing down the electron, it won't be going as slow as an electron arriving early but with the same energy as the center electrons, which is what was assumed in my calculations.

## 2.2 Beam Dynamics Simulations

### 2.2.1 General Set-Up

General Particle Tracer (GPT) was used to simulated the beam, starting at the beginning of the injection line and going all the way to the diagnostic box at the end of the analyzing leg, DB1. It was necessary to simulate the entire

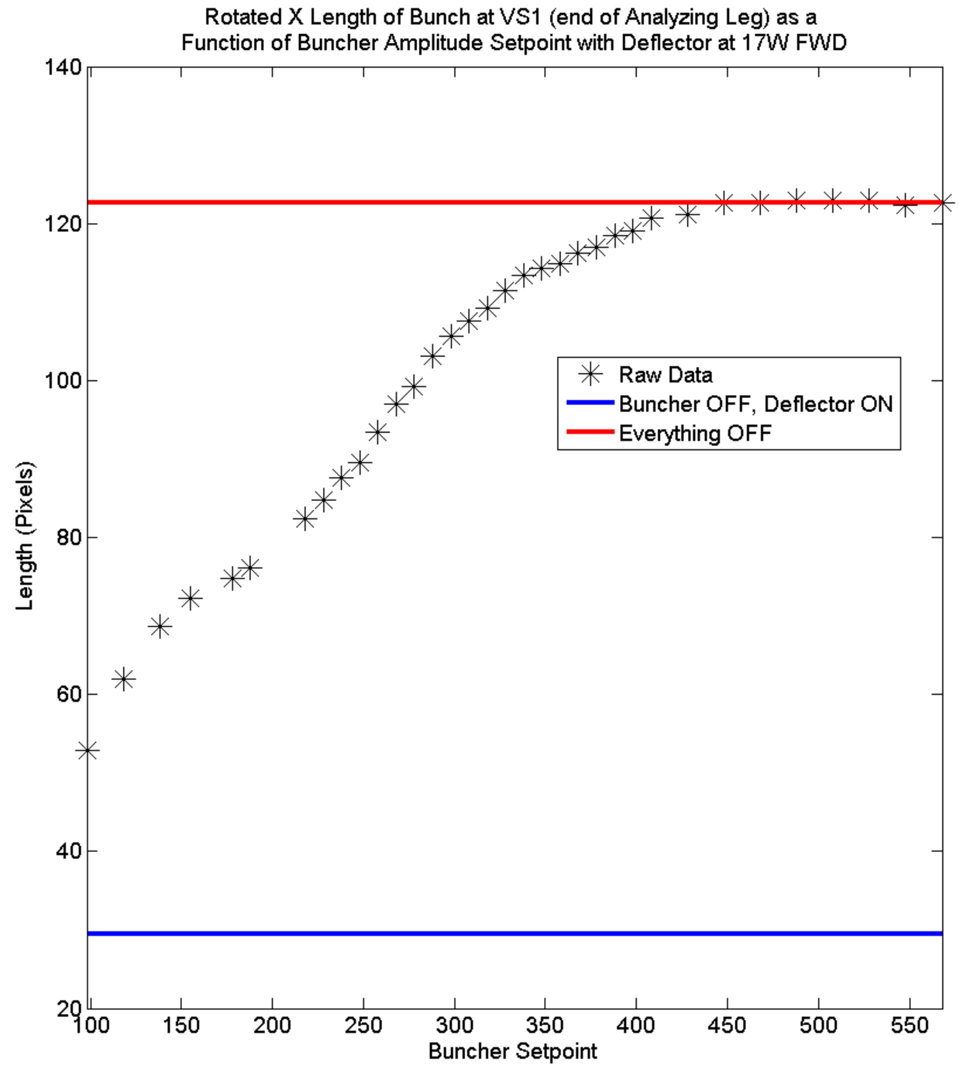


Figure 2.9: The rotated x length (in pixels) as the buncher setpoint is increased.

beamline because the output on the screen at DB1 is not only a function of the buncher, dipole magnet and deflector cavity, but also the various other elements in the beamline. The effects of one element on the beam will propagate down the entire line and must be considered.

GPT is a software package to study 3D charged beam dynamics in electromagnetic fields. The package consists of the GPT executable, which does all of the number crunching, as well as various pre- and post-processing tools to analyze and display the data. In particular, the Windows version includes a graphical user interface to facilitate running the batch files and viewing the results which are stored in a custom binary file.

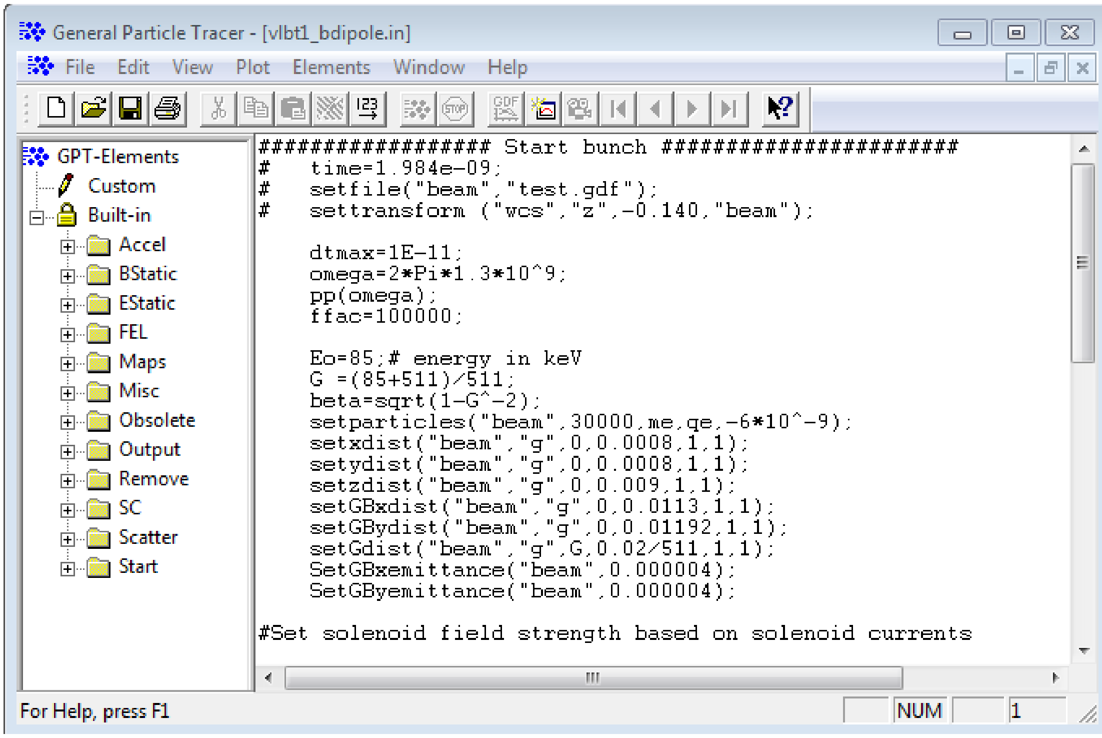


Figure 2.10: The GPT User Interface

### 2.2.2 Input Parameters

To determine the beam profile at the output we must first enter the beam characteristics as the electron bunch leaves the gun. This includes the average and standard deviation in the x, y and z directions of the beam, which is assumed to be a Gaussian distribution of particles. Instead of writing the standard deviation in z, however, in the GPT simulation the distribution of the beam is given in time instead (which is related to z by the speed of the electrons). The initial time spread of the beam depends on the experimental settings, and was about 16 degrees of 650MHz, or 68ps, in our experiment. We also need to know the average and standard deviation in the momentum in the x, y and z direction, and finally the normalized emittance in the x and y directions, $\epsilon_N x$ and $\epsilon_N y$, a measure of the area of the beam in phase space.

Unfortunately, a simulation of the electron gun output at 85keV and with the most recent modifications to the gun design has not been conducted, so instead the input parameters listed below are for a 100keV beam, with a slightly smaller cathode than the gun currently has. Table 2.1 describes the input parameters used in the GPT model.

### 2.2.3 RF Fields

In the GPT simulation, there are pre-defined elements that can be used to model resonant cavities with time dependent, user defined fields. We used these elements for the buncher and deflector cavities, obtaining the field profiles from

Table 2.1: Input Parameters for the GPT Simulation

| Name | Value | Unit |
|---|---|---|
| Conduction Angle | 16 | $^\circ$ |
| $x$ | 0 | mm |
| $y$ | 0 | mm |
| $t$ | 0 | ps |
| $\beta x$ | 0 | - |
| $\beta y$ | 0 | - |
| $\beta z$ | 0.5147 | - |
| $\sigma x$ | 0.621286 | mm |
| $\sigma y$ | 0.619437 | mm |
| $\sigma t$ | 68 | ps |
| $\epsilon_N x$ | 1.32 | mm-mrad |
| $\epsilon_N y$ | 1.30 | mm-mrad |
| $\sigma E$ | 0.293365 | keV |

RF simulations done using CST Microwave Studio. The fields obtained from CST Microwave Studio are normalized to a cavity energy of 1J. We want to multiply these fields by a field multiplication factor based on the actual cavity energy. This can be determined using equation 2.1.

$$\frac{R_{sh}}{Q} = \frac{V^2}{\omega U} \tag{2.1}$$

The geometry factor for the deflecting cavity is $R_{sh}/Q = 196\Omega$. Therefore the cavity voltage for an energy of 1J is $V_{1J}$=1.79MV. Similarly, for the buncher cavity the geometry factor is $R_{sh}/Q = 167\Omega$ and the cavity voltage for an energy of 1J is $V_{1J}$=1.65MV.

Our field multiplication factor, F, used in the GPT simulations is then given in terms of the cavity power as:

$$F = \frac{\sqrt{P_{cav} \cdot R_{sh}}}{V_{1J}} \tag{2.2}$$

### 2.2.4 Running the Code

Having modeled all of the relevant injection line optics elements in the GPT simulation, it was necessary to set up the simulation exactly as it was in the actual beam loaded tests. This involved placing collimators at the appropriate points in the simulated beamline, and setting the solenoid magnetic fields based on the solenoid current settings used.

Having done this, the code was run with the input parameters outlined in section 2.2.2 and unfortunately, on average only 0.7% of the simulated beam made it past the first two collimators. This also occurred when doing the beam loaded testing, however it caused a greater problem in the simulations, as to obtain a statistically meaningful result at the end, the number of initial particles required was too great to simulate in a reasonable timeframe.

This problem could be avoided by running the experiment in two stages. The first stage goes from the start of the beamline to the start of the dipole. The outputs from this stage, beam statistics at the start of the dipole magnet, are then transferred via a MATLAB script to another batch script which uses the results as the model for a much larger distribution of particles. This new distribution acts as the input of the second stage of the simulation which extends from the start of the dipole to the end of the analyzing leg. See Appendix D for the GPT code used.

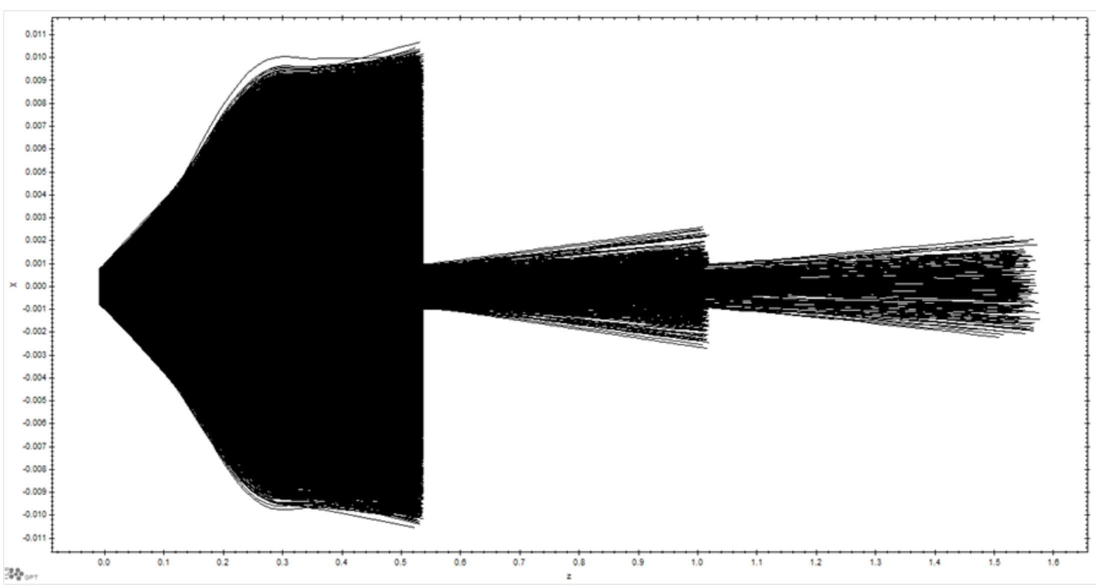

Figure 2.11: The simulated trajectory of the beam before the dipole. Note the significant loss of particles due to the collimators in place.

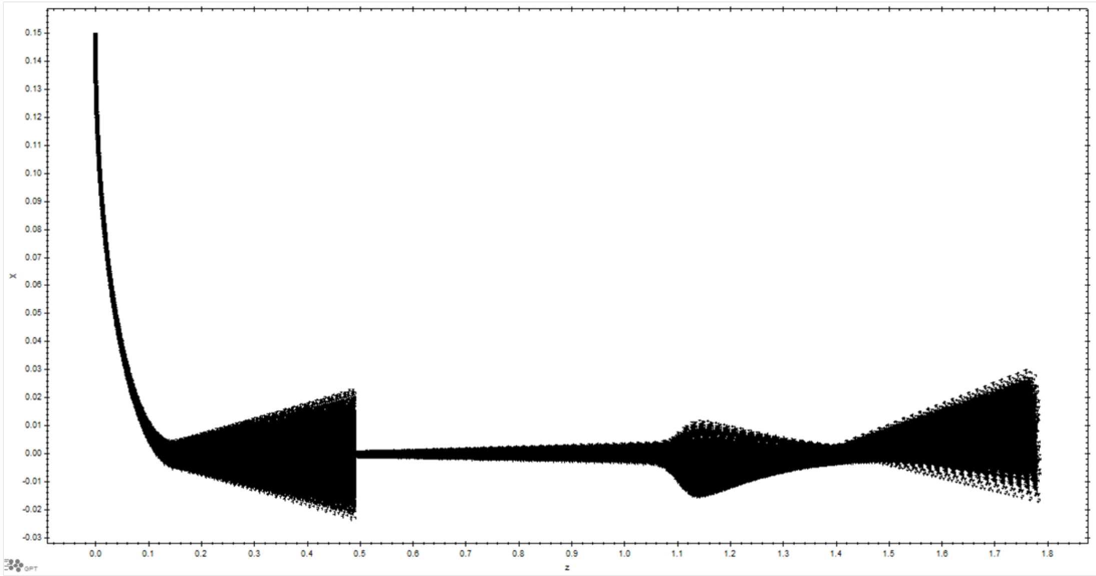

Figure 2.12: The simulated trajectory of the beam starting at the dipole. Note the effect of the dipole, bending the beam by 90°.

### 2.2.5 Simulation Results

#### Deflector Cavity

Simulations were first done using solely the deflector cavity, some results of which are shown in figure 2.13. Comparing with figure 2.3, we can see that qualitatively, we have the same beam shape and orientation in our GPT screen output as in the output from the real screen at DB1. This very promising result confirms that the model we are using for the experimental set-up in GPT matches fairly closely the actual set-up.

One significant difference between reality and our simulation is that the deflector cavity model in GPT uses the theoretical shunt impedance, and what we want to determine is the effective shunt impedance of the cavity as installed in the beamline. If we can obtain this, we will know the relationship between input power and the effective voltage of the cavity (equation 2.3).

$$V_{eff} = \sqrt{P_{in} \cdot R_{eff}} \tag{2.3}$$

This, in turn, will provide the relationship between the beam bunch length before the deflector, and the measured vertical spread at DB1:

$$\Delta y = f(V_{eff}, \Delta t) \tag{2.4}$$

To obtain this effective shunt impedance, we need to find the simulated deflector cavity power that gives us the same magnitude of vertical spread at DB1

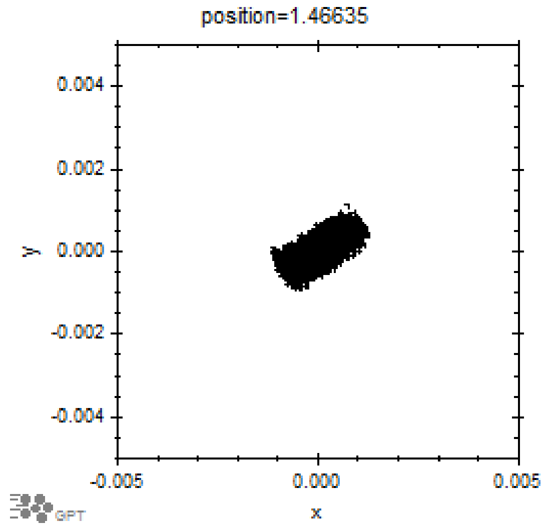


(a) Beam with no RF devices on

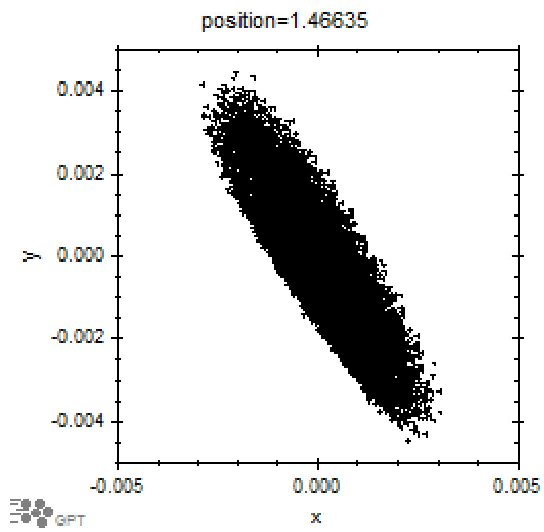


(b) Deflector at 8.5W, at the deflecting phase

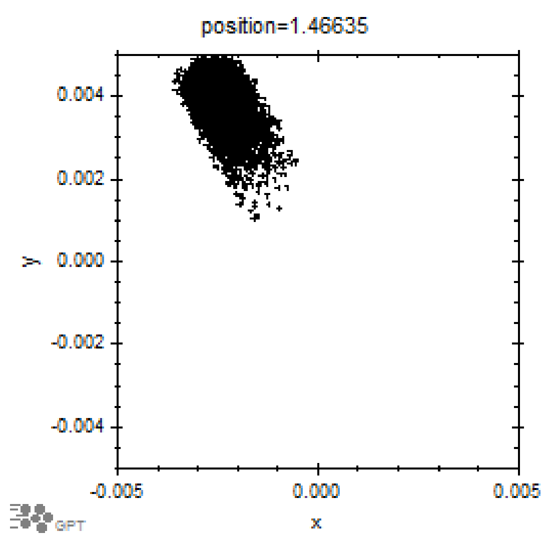


(c) Deflector at 8.5W, 90° from the deflecting phase

Figure 2.13: GPT Simulation Results: Effect of the deflector on screen output at DB1

as was measured in the real injection line. By running simulations at several different powers, it was determined that the simulated input power which produces the closest results was 16.8 W. Table 2.2 compares the beam parameters at the virtual (GPT) screen and the real screen.

Table 2.2: Comparison of GPT output and experimental results at DB1 for the deflecting phase

| Name | GPT | Experimental | Unit |
|---|---|---|---|
| Input Power | X | 8.5 | W |
| $\Delta y$ | 4.3 | 4.3 | mm |
| $\Delta x$ | 1.0 | 1.1 | mm |

Knowing that an actual input power of 8.5W corresponds to a theoretical input power of $P_{sim}$ = 16.8W, and that the theoretical shunt impedance for a $\beta = 0.51$ electron of the deflector is $R_{sim}$=1.6MΩ (1P definition), we can determine the effective shunt impedance of our actual cavity using the relationship in equation 2.5. This gives an effective shunt impedance of 0.81 MΩ.

$$P_{in}R_{eff} = P_{sim}R_{sim} \tag{2.5}$$

There are several reasons that the effective shunt impedance of our cavity is much lower than our theoretical shunt impedance. The geometry of the cavity is slightly different from the cavity model used in GPT, which is mainly due to adjustments made when tuning the cavity to the correct resonant frequency. The quality factor of the cavity is also much lower than the theoretical value of 10, 000 and was last measured as 5400.

While I have not calculated error bounds for this value as it is a first estimate and we would require more data to obtain proper error bounds, it is important to point out that this number will never be quite accurate either, due to differences in the beam parameters in real life and in the GPT simulation. While I tried to copy the experimental set-up exactly in GPT, there will undoubtedly be differences, resulting in the input voltage of the cavity needing to be slightly different to get the same deflection. However, this estimate should be a reasonable starting point for further data collection.

### The Buncher Cavity

Figure 2.14 demonstrates some results from the GPT simulation with the deflector turned on and the buncher off, at nominal power, and finally at a higher

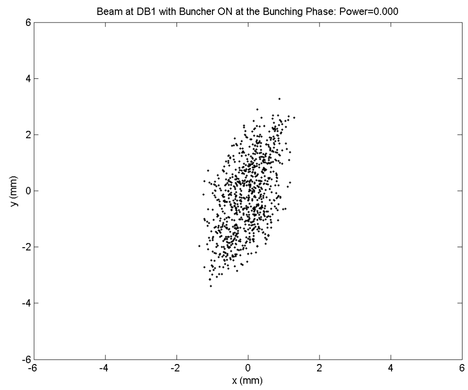


(a) Buncher OFF

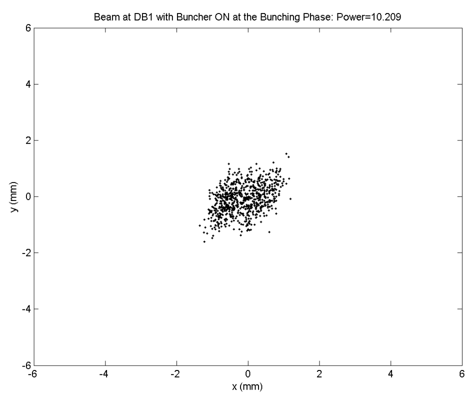


(b) Buncher at 10.2W (Nominal Power)

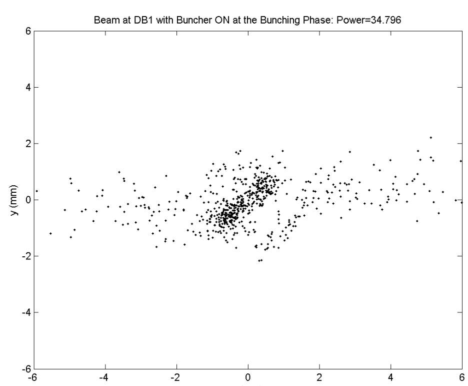


(c) Buncher at 35W

Figure 2.14: GPT Simulation Results- Effect of the buncher operating in the bunching phase on the screen output at DB1.

power. We can see that at the nominal power, the spread in the y direction is minimized, and then moving to a higher power, the vertical spread is increased again, reflecting the fact that the buncher is over-focusing.

We have already determined experimentally what the nominal buncher power is for optimal focusing at the deflector. By comparing this nominal bunching power with the value determined using the GPT simulation, we can determine the effective shunt impedance of the bunching cavity, exactly as was done with the deflector cavity in the preceding section. This was determined to be 10.2W±1.6W in the GPT simulation. The error in this number could be reduced with further simulations.

Comparing this value with our experimentally determined value of 48.5W, this is significantly lower. This discrepancy arises from several factors, including the fact that space charge (the repulsion between like charges) is neglected in the current GPT model. This will have a large effect on bunching as more power will be required to focus the electrons when space charge is considered. Similarly to the deflector, there is also the fact that the actual RF characteristics of the buncher (Q factor, geometry factor) are not the ideal values used in the GPT simulation.

Finally, with the values for the actual and simulated input power required for optimal bunching, we can determine that the effective shunt impedance of the bunching cavity is 0.326 MΩ using equation 2.5 again. Knowing the effective shunt impedance, we can use this to determine the input power required to obtain optimal focusing (minimized bunch length) for any point along the beamline.

Once again, there are no error bounds provided on this value, as not enough data is available. However, this value can now be used to focus further data collection in the right range of buncher input powers.

# Chapter 3

# Conclusions

This project set out to measure the beam bunch length for the ARIEL electron linear accelerator. This required determining the RF characteristics, in particular the effective shunt impedance, of the deflector cavity which in turn provides a relationship between vertical spread after the deflector and bunch length. In addition, work was done to determine the effective shunt impedance of the bunching cavity, so as to provide a relationship between the optimal focusing distance and input power.

To accomplish these objectives, a significant part of this project was setting up the experimental apparatus. This involved adjusting the settings of the beam optics and RF devices in the injection line, as well as inserting collimators to obtain a tightly focused beam at the diagnostic box used for data collection. The experimental procedure was provided by Bob Laxdal, the project sponsor, and was then adjusted as the data collection proceeded. Both the experimental set-up and procedure developed during this project will be useful when taking further data collection. In addition, the tools developed while analyzing the data such as the GPT simulation, will be relevant for future work on this project as well as other projects relating to the injection line.

Having collected and analyzed the first round of data, the effective shunt impedance of the deflecting cavity as installed in the beamline was determined to be 0.81M$\Omega$. This is significantly different than the ideal shunt impedance of 1.6M$\Omega$, but this is expected due to differences in the computer model of the deflector and the actual deflector cavity. Error bounds are not available for this value, but can and should be obtained by collecting more data points. The value obtained for the effective shunt impedance can then be used to determine the relationship between vertical spread at DB1 and bunch length. This will allow us to use the deflector cavity as a powerful diagnostic device, giving us the length of the beam bunch in the injection line. Such a measurement is important for accelerator engineers in optimizing the acceleration and focusing of the beam, as well as to downstream users who require this type of information when conducting their experiments.

The effective shunt impedance of the buncher cavity was determined to be

0.326M$\Omega$, compared with a simulated (theoretical) value of 1.55M$\Omega$ for a $\beta = 0.51$ particle. The discrepancy in this value is expected not only due to differences in the ideal buncher and the buncher as installed in the beamline, but also due to the absence of effects such as space charge in the current GPT simulation model. The repulsion between electrons will mean that we expect to obtain a lower shunt impedance as it is harder to focus the electron bunch. We can use this value for the shunt impedance to determine the power required for optimal focusing of the bunch at any point in the beamline, allowing us to provide small, tightly concentrated bunches of electrons to users downstream, a desirable quality in a beam.

# Chapter 4

# Project Deliverables

The following deliverables are to be transferred to the project sponsor. Note that the results obtained are a first estimate, and should be confirmed with further data collection (see chapter 5).

1. Effective shunt impedance of the buncher cavity
2. Effective shunt impedance of the deflector cavity
3. General Particle Tracer simulation code and results
4. The raw experimental data collected
5. All other plots, images and animations resulting from the data collection and analysis
6. A final report documenting the project, including recommendations for future work

# Chapter 5

# Recommendations

While a significant amount of work has been accomplished in the last four months, there is still much to do to obtain a robust program for beam bunch length measurement, as well as to fully characterize the bunching cavity, necessary for optimal temporal focusing of the bunch. Now that the groundwork has been laid, future work can build on this to solidify the results obtained and apply them in a useful manner.

1. One of the main objectives achieved during this project was the development of the experimental set-up and procedure. In conjunction with the data analysis tools developed during the project (GPT simulations, MATLAB scripts, etc), this has greatly facilitated data collection and analysis. With the framework in place, this project is at the stage where more data should be collected to confirm the results obtained, and set error bounds on these values.

2. The GPT input beam parameters are not actually up to date, and were obtained using an older gun design. While it was assumed that the differences in beam characteristics would be small, it would be beneficial to obtain the most up to date results from the electron gun simulations.

3. The original objective of this project was to produce a computer program that could analyze an image and in combination with user input of some of the RF and beam parameters, the program would output the beam bunch length. The results of this project have brought us much closer to this objective by characterizing the RF cavities involved and providing a relationship between the spread in time and the vertical smear after the deflector. The next step would be to use these results in developing this program.

4. As part of the analysis, it would be convenient to determine the relationship between the current of the solenoid after the deflector, VLBT1 SOL1, and the rotation of the beam axes. This may not be possible if this relationship depends on the beam properties, but it could be worth investigating. In particular, if this relationship were determined, it could be used in conjunction with the new feature in the viewscreens that allows the user to rotate the images obtained.

# Chapter 6

# Acknowledgments

This project is part of a much larger goal to characterize the entire VECC injection line, and as such I had the opportunity to work with several accelerator physicists and engineers at TRIUMF while completing this project. I would like to thank all of these individuals for the incredible amount of assistance and guidance I received and acknowledge their crucial role in the completion of this project. Without their contributions, from characterizing the solenoids to helping me take data to reviewing my work, I could not have completed any of this. In particular, I would like to thank:

- Bob Laxdal, head of the superconducting RF group at TRIUMF, who has been an excellent supervisor, providing inspiration and much guidance and expertise throughout the project.

- Chris Gong, graduate student at TRIUMF, who assisted in the collection of data and was always on hand to discuss questions pertaining to beam optics and the GPT simulations.

- Yu-Chiu Chao, beam optics researcher at TRIUMF, who is spearheading the initiative to characterize the VECC beamline elements and was thus an important contributor to the project in providing the input parameters for the GPT simulations as well as the models for some of the other beamline elements.

- Vladimir Zvagintsev, SRF Engineering at TRIUMF, designed the deflector cavity and provided the electromagnetic field distribution results from RF simulations of the cavity, which are necessary for the beam dynamics simulations. He was also on hand to answer questions regarding the deflector and buncher cavities.

- Philipp Kolb, graduate student at TRIUMF, has proven very useful for bouncing ideas off of and answering endless questions.

I also greatly appreciated the support of the electrical, EPICS, and low level RF groups at TRIUMF.

# Bibliography


[1] Belomestnykh, S., Bazarov, I., Shemelin., V. Sikora, J., Smolenski, K., Veshcherevich, V. " Deflecting Cavity for Beam Diagnostics at Cornell ERL injector", *Nuclear Instruments and Methods in Physics Research A*, vol. 614, 2010, pages 179-183.

[2] Fliller, R., Edwards, H., Ruan, J. " Start to End Simulations of Transverse to Longitudinal Emittance Exchange at the A0 Photoinjector", *Proceedings of EPAC08, Genoa, Italy*, 2008, pages 3002-3004.

[3] Mastuba, S., Honda, Y., Miyajima, T. "Deflecting Cavity for Bunch Length Diagnostics at Compact ERL Injector", *Proceedings of IPAC'10, Kyoto, Japan*, pages 951-953.

[4] Shemelin, V., Belomestnykh, S. "RF Design of the Deflecting Cavity for Beam Diagnostics in ERL Injector", *http://www.lns.cornell.edu/public/ERL/2007/ERL07-2/ERL07-2.pdf*, 2007.

[5] Zhou, F., Adolphsen, C., Ding, Y., Li, Z., Vlieks, A. " X-Band Photoinjector Beam Dynamics", *Proceedings of IPAC'10, Kyoto, Japan*, 2010.

# Appendix A

# Buncher Cavity Power Calculations

# Buncher Power Determination

For a buncher with shunt impedance, $R_{sh}$, and transit time factor, $T_0$, we can determine the approximate power required for optimal focusing after a given drift length.

In the operational mode, RF electric fields propagating in the buncher are in the z direction (direction of travel of the beam), and have a sinusoidal time dependence. We only want to operate in the ascending, linear region of the sinusoidal wave, as depicted by figure 1. Electrons that are lagging behind the center of the bunch will undergo positive acceleration, while leading electrons will be decelerated.

Figure 1: Operating RF Regime of Buncher Cavity

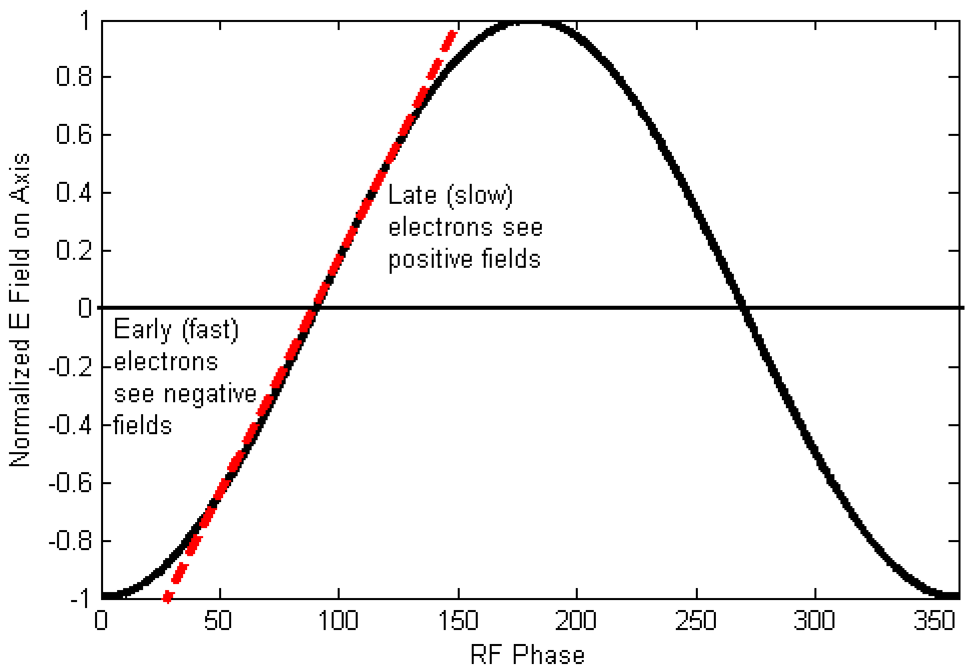


To optimize the buncher we want the particles at the extremities of the bunch to undergo acceleration such that by the end of the subsequent drift, $d$, the beam is focused in the longitudinal direction. The particle at the center of the beam undergoes no acceleration, so $\beta = \beta_0$. Let's consider the voltage required for an electron at a phase offset of $\phi_0$ (relative to the RF of the buncher) from the center of the beam to reach the point $d$ in the same time as the center of the bunch. Start by solving for the $\beta$ required. Initially the longitudinal spread is given by:

$$\Delta L = \frac{\phi_0}{\omega_0} * \beta_0 c \tag{1}$$

Where $\omega_0$ is the resonant frequency of the bunching cavity. For $\Delta L$ to be 0 by the end of a drift, $d$, we need (assuming we are using a sin wave and that the middle of the bunch reaches the buncher at $\phi = 0$):

$$t_{travel}|_{\phi=0} = \Delta t + t_{travel}|_{\phi_0} \tag{2}$$

$$\Rightarrow \frac{d}{\beta_0 c} = \frac{d}{\beta c} + \frac{\phi_0 \beta_0 c}{\omega_0 \beta c} \tag{3}$$

Solving for $\beta$ gives:

$$\beta = \beta_0 + \frac{\phi_0 c \beta_0^2}{\omega_0 d} \tag{4}$$

Given $\beta$, we can find the change in energy required:

$$\begin{aligned}\frac{\Delta E}{E} =& (\beta_0\gamma_0)^2 \frac{\beta - \beta_0}{\beta_0} \\ =& (\beta_0\gamma_0)^2 \frac{\phi_0 \beta_0 c}{\omega_0 d} \end{aligned} \tag{5}$$

The change in energy of a particle in an electric field, $\Delta E$, in eV, is given by the voltage, $V$. We can determine the required $V_{eff}$, making the following approximation as we are operating in the linear regime of the sinusoid:

$$V = V_{eff} \sin \phi_0 \approx \phi_0 V_{eff} \tag{6}$$

$$\Rightarrow V_{eff} = \frac{\Delta E}{\phi_0} \tag{7}$$

$$\Rightarrow V_{eff} = (\beta_0\gamma_0)^3 E_0 \frac{c}{\omega_0 d} \tag{8}$$

For our buncher, $\omega_0 = 2\pi \cdot 1.3\text{E}9$, and with the current experimental setup, $E_0 = 511keV$, $\beta_0 = 0.5147$, $\gamma_0 = 1.166$ and our drift length is the distance from the buncher to the deflector cavity (where we are actually measuring the time spread, even if the result only shows up at the diagnostic box after the deflector). This distance is $d = 1.53m$, assuming a perfect trajectory (centered). Substituting these values into equation 8, we find that our required effective voltage is approximately 2.65kV.

Having solved for the effective voltage, we need to convert this to the actual required cavity voltage, $V_0$ which will depend on the transit time factor of the cavity, $T_0$:

$$V_0 = \frac{V_{eff}}{T_0} \tag{9}$$

$$\Rightarrow T_0 = \frac{\int_{-\infty}^{\infty} E(\rho = 0, z) \exp(i\omega_0 \frac{z}{\beta c}) \, \mathrm{d}z}{\int_{-\infty}^{\infty} E(\rho = 0, z) \, \mathrm{d}z} \tag{10}$$

This transit time factor will depend on the speed of the electrons. Using equation 10, and substituting in the values mentionned above, we obtain T=0.82 for a $\beta = 1$ particle, and T=0.47 for a $\beta = 0.5147$ electron.

Finally, we can use the shunt impedance to find the required input power to the cavity. Note this needs to be divided by 2 if $R_{sh}$ is given using the 2P definition.

$$P_{in} = \frac{V_0^2}{R_{sh}} \tag{11}$$

The shunt impedance for this buncher cavity (EMMA buncher) was determined experimentally to be 3.27MΩ using the 2P definition. Therefore, the nominal bunching power required for optimal focusing of the bunch at the deflector cavity is:

$$P_{in} = \frac{V_0^2}{2R_{sh}} = \frac{(5.64\text{kV})^2}{2 \cdot 3.27\text{E}6\ \Omega} = 4.87\text{W} \tag{12}$$

# Appendix B

# Beam Optics Settings for Data Collection

Time: Mon Nov 26 19:00:57 2012
Login ID: veccops (VECC Ops User)
Eff UID: 1372
Group ID: 24
Keywords:
Comments:
Type: Absolute
Directory /epicsserver/usr1/local/epics/projects/vecc
Req File: /usr1/vecc/burt/vecc.req

RO VGUN:BIAS1:RDCUR.VAL 1 1.367208361943999e-02
RO VGUN:BIAS1:RDVOL.VAL 1 8.505378805218586e+04
RO VGUN:BIAS1:DRVBIT.RVAL 1 1.000000000000000e+00
VGUN:BIAS1:VOL.VAL 1 8.500000000000000e+04
RO VGUN:CHT:RDCUR.VAL 1 1.263980463980464e+03
RO VGUN:CHT:RDVOL.VAL 1 6.520146520146520e+00
VGUN:CHT:VOL.VAL 1 6.399999999999999e+00
VGUN:CHT:CUR.VAL 1 1.485720000000000e+03
RO VGUN:CATHB:RDCUR.VAL 1 2.122100122100122e+00
RO VGUN:CATHB:RDVOL.VAL 1 1.015873015873016e+02
VGUN:CATHB:VOL.VAL 1 1.000000000000000e+02
VGUN:CATHB:CUR.VAL 1 5.042700000000000e+00
RO VLBT:XCB1A:RDCUR.VAL 1 -6.843671320668346e-02
RO VLBT:XCB1A:RDVOL.VAL 1 -3.854428931105516e-01
RO VLBT:XCB1A:DRVBIT.RVAL 1 0.000000000000000e+00
VLBT:XCB1A:CUR.VAL 1 -5.999999999999989e-02
RO VLBT:YCB1A:RDCUR.VAL 1 6.996261539635310e-02
RO VLBT:YCB1A:RDVOL.VAL 1 1.657129777981231e-01
RO VLBT:YCB1A:DRVBIT.RVAL 1 0.000000000000000e+00
VLBT:YCB1A:CUR.VAL 1 9.000000000000000e-02
RO VLBT:SOL1:RDCUR.VAL 1 8.704509040970474e-01
RO VLBT:SOL1:RDVOL.VAL 1 7.427786678873884e+00
RO VLBT:SOL1:DRVBIT.RVAL 1 1.000000000000000e+00
VLBT:SOL1:CUR.VAL 1 8.699999999999999e-01
RO VLBT:XCB1B:RDCUR.VAL 1 -1.266498817425803e-02
RO VLBT:XCB1B:RDVOL.VAL 1 -2.915999084458686e-01
RO VLBT:XCB1B:DRVBIT.RVAL 1 0.000000000000000e+00
VLBT:XCB1B:CUR.VAL 1 -3.000000000000003e-02
RO VLBT:YCB1B:RDCUR.VAL 1 -1.057450217441062e-01
RO VLBT:YCB1B:RDVOL.VAL 1 -9.750514991989014e-02
RO VLBT:YCB1B:DRVBIT.RVAL 1 0.000000000000000e+00
VLBT:YCB1B:CUR.VAL 1 -1.999999999999999e-02
RO VLBT:SOL2:RDCUR.VAL 1 -1.358052948805982e-02
RO VLBT:SOL2:RDVOL.VAL 1 -1.496910048065919e-01
RO VLBT:SOL2:DRVBIT.RVAL 1 1.000000000000000e+00
VLBT:SOL2:CUR.VAL 1 -1.000000000000082e-02
RO VLBT:XCB2:RDCUR.VAL 1 1.149004348821241e-01

RO VLBT:XCB2:RDVOL.VAL 1 4.623483634699016e-02
RO VLBT:XCB2:DRVBIT.RVAL 1 0.000000000000000e+00
VLBT:XCB2:CUR.VAL 1 2.400000000000000e-01
RO VLBT:YCB2:RDCUR.VAL 1 -5.630579079880980e-02
RO VLBT:YCB2:RDVOL.VAL 1 -9.933623254749371e-02
RO VLBT:YCB2:DRVBIT.RVAL 1 0.000000000000000e+00
VLBT:YCB2:CUR.VAL 1 -3.000000000000002e-02
RO VLBT:SOL3:RDCUR.VAL 1 3.509575036240177e-03
RO VLBT:SOL3:RDVOL.VAL 1 1.835660334172579e-01
RO VLBT:SOL3:DRVBIT.RVAL 1 0.000000000000000e+00
VLBT:SOL3:CUR.VAL 1 2.999999999999958e-02
RO VLBT:XCB3A:RDCUR.VAL 1 -8.158999008163577e-01
RO VLBT:XCB3A:RDVOL.VAL 1 -5.699244678416113e-01
RO VLBT:XCB3A:DRVBIT.RVAL 1 0.000000000000000e+00
VLBT:XCB3A:CUR.VAL 1 -9.350000000000003e-01
RO VLBT:YCB3A:RDCUR.VAL 1 -2.186617837796597e-01
RO VLBT:YCB3A:RDVOL.VAL 1 -1.661707484550240e-01
RO VLBT:YCB3A:DRVBIT.RVAL 1 0.000000000000000e+00
VLBT:YCB3A:CUR.VAL 1 -3.399999999999998e-01
RO VLBT:FC0V:SCALECUR.VAL 1 0.000000000000000e+00
VLBT:FC0V:GAIN.RVAL 1 1.000000000000000e+00
VLBT:FC0V:RDVOL.SMOO 1 0.000000000000000e+00
RO VLBT:FC1AV:SCALECUR.VAL 1 -6.347849971007416e-08
RO VLBT:FC1A:STATON.RVAL 1 0.000000000000000e+00
VLBT:FC1AV:GAIN.RVAL 1 6.000000000000000e+00
VLBT:FC1AV:RDVOL.SMOO 1 0.000000000000000e+00
RO VLBT:FC1B:STATON.RVAL 1 0.000000000000000e+00
RO VLBT:FC3V:SCALECUR.VAL 1 4.882961516159551e-09
RO VLBT:FC3:STATON.RVAL 1 0.000000000000000e+00
VLBT:FC3V:GAIN.RVAL 1 1.200000000000000e+01
VLBT:FC3V:RDVOL.SMOO 1 0.000000000000000e+00
RO VLBT:BPM1A:X.VAL 1 -4.619000000000000e+00
RO VLBT:BPM1A:Y.VAL 1 -2.793000000000000e+00
RO VLBT:BPM1A:INTENSITY.VAL 1 6.808800000000001e+01
RO VLBT:BPM1A:ERROR.VAL 1 0.000000000000000e+00
RO VLBT:BPM1B:X.VAL 1 -3.011000000000000e+00
RO VLBT:BPM1B:Y.VAL 1 -6.770000000000000e-01
RO VLBT:BPM1B:INTENSITY.VAL 1 5.409800000000000e+01
RO VLBT:BPM1B:ERROR.VAL 1 0.000000000000000e+00
RO VLBT:IG1:RDVAC.VAL 1 1.248702831369807e-08
RO VLBT:IG1:STATDRV.RVAL 1 1.000000000000000e+00
RO VLBT:IG2:RDVAC.VAL 1 1.969070629206549e-08
RO VLBT:IG2:STATDRV.RVAL 1 1.000000000000000e+00
RO VLBT:IG3:RDVAC.VAL 1 9.999999999999999e-12
RO VLBT:IG3:STATDRV.RVAL 1 0.000000000000000e+00
RO VEMIT:IG1:RDVAC.VAL 1 5.252798246288538e-09
RO VEMIT:IG1:STATDRV.RVAL 1 1.000000000000000e+00

```
VLBT:BUNCH1:ASET.VAL 1 2.280000000000000e+02
VLBT:BUNCH1:PSET.VAL 1 -4.621760000000000e+01
RO VLBT1:MB0:RDCUR.VAL 1 4.531929503318837e-02
RO VLBT1:MB0:RDVOL.VAL 1 4.206912336919204e-01
RO VLBT1:MB0:DRVBIT.RVAL 1 0.000000000000000e+00
VLBT1:MB0:CUR.VAL 1 0.000000000000000e+00
RO VLBT1:YCB0A:RDCUR.VAL 1 1.525902189669637e-04
RO VLBT1:YCB0A:RDVOL.VAL 1 4.577706569008910e-04
RO VLBT1:YCB0A:DRVBIT.RVAL 1 0.000000000000000e+00
VLBT1:YCB0A:CUR.VAL 1 0.000000000000000e+00
RO VLBT1:XCB0B:RDCUR.VAL 1 -3.462272068360418e-01
RO VLBT1:XCB0B:RDVOL.VAL 1 -2.623025864042115e-01
RO VLBT1:XCB0B:DRVBIT.RVAL 1 0.000000000000000e+00
VLBT1:XCB0B:CUR.VAL 1 -4.000000000000000e-01
RO VLBT1:YCB0B:RDCUR.VAL 1 -3.341725795376516e-02
RO VLBT1:YCB0B:RDVOL.VAL 1 -8.194094758525979e-02
RO VLBT1:YCB0B:DRVBIT.RVAL 1 0.000000000000000e+00
VLBT1:YCB0B:CUR.VAL 1 -1.263999999999994e-01
RO VLBT1:SOL1:RDCUR.VAL 1 1.268482490272373e+00
RO VLBT1:SOL1:RDVOL.VAL 1 2.271915770199130e+00
RO VLBT1:SOL1:DRVBIT.RVAL 1 1.000000000000000e+00
VLBT1:SOL1:CUR.VAL 1 1.300000000000000e+00
RO VLBT1:FC0V:SCALECUR.VAL 1 0.000000000000000e+00
RO VLBT1:FC0:STATON.RVAL 1 0.000000000000000e+00
VLBT1:FC0V:GAIN.RVAL 1 2.400000000000000e+01
VLBT1:FC0V:RDVOL.SMOO 1 0.000000000000000e+00
RO VLBT1:FC1V:SCALECUR.VAL 1 0.000000000000000e+00
RO VLBT1:FC1:STATON.RVAL 1 0.000000000000000e+00
VLBT1:FC1V:GAIN.RVAL 1 4.800000000000000e+01
VLBT1:FC1V:RDVOL.SMOO 1 0.000000000000000e+00
RO VLBT1:IG1:RDVAC.VAL 1 1.465737388299312e-07
```

# Appendix C

# Experimental Procedure

# Experimental Procedure- Deflector and Buncher RF Characterization

**Authors: Bob Laxdal, Alysson Vrielink, Chris Gong, Yu Chiu Chao**

November 26th, 2012

1. With the RF deflector and RF buncher off establish a beam with low transverse emittance around the analyzing leg:

    a. Choose a relatively high cathode bias to reduce the conduction angle (~100V) and a high duty cycle (~10%-20%).

    b. Align the beam and ensure it is parallel using DB1A and DB1B.

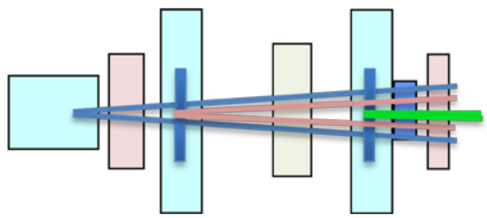

    c. Insert the 1mm radius circular collimators (xy slits) at DB1A and DB1B and use SOL1A, SOL1B and VLBT1:SOL1 to collimate the beam –optimize dipole magnet for maximum transmission to VLBT1:DB1 (~168mA). The optics settings used on November 26th, which proved effective, can be found using the save restore feature and loading 121126_1953-vecc.snap.

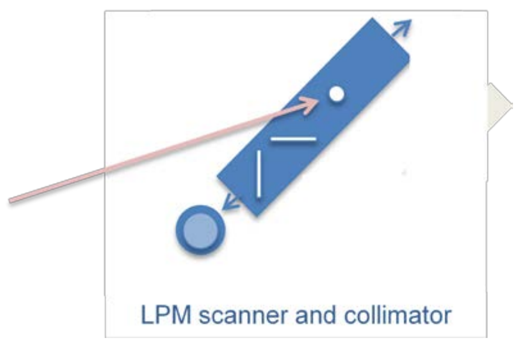


    d. With the collimators in, increase the RF level until high enough current is obtained at FC1 on the analyzing leg but less than 1uA.

    e. Insert the screen at VLBT1:DB1. Adjust VLBT1:SOL1 for best beam spot on the screen.

2. Setting up the deflector:

    a. The LPM0 x-slit can be inserted (position at around 146.5mm) to select a certain energy slice if desired.

    b. Turn on deflector to nominal power (see deflector operating procedure) at ~50W, including the 3dB loss in input cable. Scan phase to identify the deflecting and non deflecting phases using the screen. The non deflecting phase is the phase at which the y spread in the beam is minimized. Note: with VLBT1:SOL1 on, the x-y axis is rotated.

c. Scanning through the phase, take screenshots every 30 degrees.

d. Repeat steps b) and c) for several power levels (although the deflecting phase should be independent of input power).

3. Setting up the buncher:
   a. Make sure the LPM0 x-slit isn't inserted if the intent is to look at the effect of the buncher on energy spread of the beam.

   b. Turn on buncher to nominal power (see buncher operating procedure) at ~48.5W, including the 1dB loss in the input cable. Scan phase to determine the accelerating and bunching phases. The accelerating phase will be evident as the point where the x centroid of the beam is farthest away from the x centroid with the buncher off. The non accelerating phases should be when the beam is at approximately the same location with the buncher off.

   c. To identify the bunching phase, turn on the deflector at the deflecting phase. The bunching phase will show far less vertical smear than the debunching phase if the buncher is close to the nominal power.

4. Determining the nominal buncher power

   a. With the deflector turned on at the nominal power and at the deflecting phase, adjust the buncher setpoint, recording the FWD and REV power as read out by the power meter connected to the buncher. Determine the setpoint where the vertical smear is minimized.

5. Longitudinal Emittance Measurements

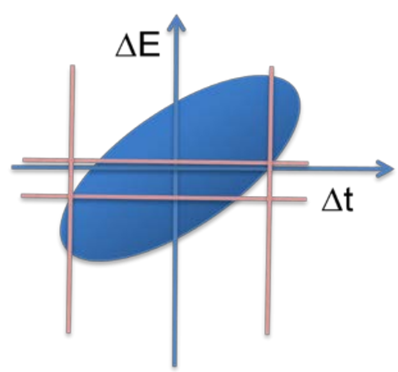


   a. Use the LPM0 slit to select a portion of the dispersed beam and use the deflector to measure the time spread

   b. For each slit position record profile with and without deflector on using the deflecting (0 degree) phase and power level determined in the initial set-up (step 2.)

# Appendix D

# GPT Code

```
################## Start bunch #######################
#   time=1.984e-09;
#   setfile("beam","test.gdf");
#   settransform ("wcs","z",-0.140,"beam");

    dtmax=1E-11;

    omega=2*Pi*1.3*10^9;
    ffac=8E3;

    Eo=85;# energy in keV
    G =(85+511)/511;
    beta=sqrt(1-G^-2);
    setparticles("beam",15000,me,qe,-6*10^-9);
    setxdist("beam","g",0,0.000621286,2,2);
    setydist("beam","g",0,0.000619437,2,2);
    settdist("beam","u",0, 6.8E-11);
    setGBxdist("beam","g",0,0.0113,2,2);
    setGBydist("beam","g",0,0.01192,2,2);
    setGdist("beam","g",G,0.293365/511,2,2);
    SetGBxemittance("beam",2.5E-6);
    SetGByemittance("beam",2.5E-6);

#Set solenoid field strength based on solenoid currents

   sol1=1.03E-2;
   sol2=2.24E-4;

###################inputs#########################
   zend = 1.26;#(1.26+0.15)
   zdb1a=0.54123;
   zdb1b=zdb1a+0.48173;
   zdbvlbt10=0.34406+0.15;
   zdbvlbt11=0.46196+0.51033+zdbvlbt10;
########################################################

##################### elements############################
      map1D_B("wcs","z",0.01926,"bNW.gdf","z","Bz",sol1);

#     BUNCHER: (COMMENT TO TURN OFF)

map1D_TM("wcs","z",0.59241,"bun.gdf","z","Ez",ffac,phi*Pi/180,om
ega);

      map1D_B("wcs","z",0.91414,"bsol.gdf","z","Bz",sol2);

#     DIAGNOSTIC BOXES
```

```
        rmax("wcs","z",zdb1a,1E-3,5E-3);
        rmax("wcs","z",zdb1b,1E-3,5E-3);


#       screen("wcs","I",zdb1a-10E-3);
#       screen("wcs","I",zdb1a);

#       screen("wcs","I",zdb1b-10E-3);
#       screen("wcs","I",zdb1b);
        screen("wcs","I",zend);
        tout(0,1e-08,0.1e-09,"wcs");
```

```
################## Start bunch #######################

#Set maximum step size
    dtmax=1E-11;
#Set field factor for deflector
   ffac=2.9E-3;
#  rfphase=phi;
   rfphase=0;

#Set up beam at point right before dipole

avgGBx=avgBx*sqrt(1/(1-avgBx^2));
avgGBy=avgBy*sqrt(1/(1-avgBy^2));
avgGBz=avgBz*sqrt(1/(1-avgBz^2));

stdGBx=stdBx*(1/(1-avgBx^2))^3/2;
stdGBy=stdBy*(1/(1-avgBy^2))^3/2;
stdGBz=stdBz*(1/(1-avgBz^2))^3/2;

npar=10000;

#Assume on-axis

    Eo=85;# energy in keV
    G =(85+511)/511;
    beta=sqrt(1-G^-2);

    setparticles("beam",npar,me,qe,qe*npar);
    setxdist("beam","g",0,stdx,2,2);
    setydist("beam","g",0,stdy,2,2);
    settdist("beam","g",0,stdt,2,2);
    SetGBxdist("beam","g",avgGBx,stdGBx,2,2);
    SetGBydist("beam","g",avgGBy,stdGBy,2,2);
    SetGBzdist("beam","g",avgGBz,stdGBz,2,2);

    SetGBxemittance("beam",nemixrms);
    SetGByemittance("beam",nemiyrms);

#Set solenoid field strength based on solenoid currents

   vlbt1sol=1.8E-2;

###################inputs#########################
   energy = 85; #in keV
   gamma = (energy+511)/511 ; # value of gamma
   zend = 1.26;#(1.26+0.15)
   Rbend = 0.15; # radius of curvature of the dipole in m
```

```
   angle = 90; # bending angle in degree
   phiin =0 ; # entry cut angle
   phiout = 0 ; # exit cut angle
   dl = 0;# offset
   b1 =0; # dipole fringe field coefficient
   b2 =0; # ......do..................
   zdb1a=0.54123;
   zdb1b=zdb1a+0.48173;
   zdbvlbt10=0.34406+0.15;
   zdbvlbt11=0.46196+0.51033+zdbvlbt10;
########################################################


#We actually start at this point

# ---------------dipole magnet----------------------------------
      beta = sqrt(gamma*gamma-1)/gamma ;
      Bfield = -me*c*gamma*beta/(qe*Rbend) ;
      ccs("wcs", 0,0,0.15, cos(angle/deg),0,-sin(angle/deg),
0,1,0, "bend");
      sectormagnet("wcs","bend", Rbend, Bfield, 30/deg,30/deg,
dl, b1, b2);
#-------------------------------------------------------------
---

#      xymax("bend","z",zdbvlbt10,2E-3,1,5E-3);


#     DEFLECTOR: (COMMENT TO TURN OFF)
     map3D_TM("bend",
"z",0.51479,"TM.gdf","x","y","z","Ex","Ey","Ez","Bx","By","Bz",f
fac,rfphase*Pi/180,2*Pi*1.3*10^9);

#     VLBT1 SOLENOID
      map1D_B("bend","z",0.95602,"bsol.gdf","z","Bz",vlbt1sol);

#Switch co-ordinate frame again
angle1=-30;
ccs("bend", 0,0,zdbvlbt11, cos(angle1/deg),-sin(angle1/deg),0,
sin(angle1/deg),cos(angle1/deg),0, "new");

################################################################
#####################

#     screen("bend","I",zdbvlbt11);
     screen("bend","I",zdbvlbt11,"new");
     tout(0,1.2e-08,0.1e-09,"bend");
```

```
#screen("bend","I",zdbvlbt11);
#tout(0,1.2e-08,0.1e-09,"bend");
```